Seismic performance of a ductile rod exterior connection system for precast concrete industrial buildings

Donghyuk Jung, Thomas H.-K. Kang, Dong Joo Lee, Sanghee Kim, and James M. LaFave

- This study presents a ductile rod exterior connection system developed for applications to precast concrete pipe rack frames in industrial plants.
- Five full-scale precast concrete specimens representing T-shaped exterior joints were constructed for testing. For the purpose of comparing responses of the precast concrete connections with those of cast-in-place reinforced concrete connections, two comparable full-scale conventional reinforced concrete beam-to-column joint specimens were also constructed and tested under the equivalent lateral loading.
- Seismic performance of the developed exterior connection system was experimentally investigated through a series of quasi-static cyclic lateral loading tests.

Precast or prefabricated concrete offers great benefits, such as high construction quality, speed, and economic efficiency.[1,2] Considerable efforts have been made in recent decades to develop various types of precast concrete connection systems. Some early studies attempted to adopt welded connections for joining precast concrete beams and columns. Pillai and Kirk[3] used steel plates and bars, welded at the top and bottom ends of the beam, and tested nine full-scale precast concrete beam-to-column specimens along with two reinforced concrete specimens. Bhatt and Kirk[4] improved the detail of the previous welded connection, which showed premature joint failure, by adding T-shaped steel plates. Then, in 1987, the National Institute of Standards and Technology initiated research for the design of an earthquake-resistant and fast, constructible precast concrete connection system. Experimental testing on precast concrete and reinforced concrete beam-to-column connections was conducted in a total of four phases.[5–8] In those studies, prestressing bars and strands were used for enhanced energy dissipation of precast concrete beam-to-column connections. The use of partially bonded strands to reduce slip at the joint was also considered. In the last phase, hybrid connections that used low-strength steel bars and prestressing steel were devised for high energy dissipation as well as strong lateral resistance. In 1990, as part of a coordinated project between the United States and Japan, the PRESSS (Precast Seismic Structural Systems) research program was launched for the purpose of developing the seismic design of precast concrete structures.[9] Diverse design concepts were discussed in PCI workshops, including a spaced-out thread-bar frame system, which is a type of bolted connection that employs wrench-tight threaded bars for the beam-to-column joint.[10] The bolted-type precast concrete connection was further developed by Nakaki et al.[11] with the concept of a ductile precast concrete frame (DPCF) that uses a ductile link connector. This connector assembles beam and column components through ductile rods embedded in the column. Within the DPCF, inelastic deformation is mainly enforced in the ductile rods, inducing a plastic hinge at the column joint. A DPCF beam-to-column subassembly tested under lateral cyclic loading exhibited stable response with no strength degradation at drift ratios beyond 4% and sustained a minimal degree of structural damage.[11,12] Study of the hybrid connection was followed by experimental work at the University of Washington.[13,14] Three two-thirds scale beam-to-column assemblies connected with mild steel bars and unbonded prestressing tendons were tested under quasi-static cyclic loading. Yielding of mild steel bars and recentering of the prestressing tendons provided the precast concrete beam-to-column connections with sufficient deformation and energy dissipation capabilities with little structural damage. More recently, Chang et al.[15] conducted full-scale testing of two interior precast concrete beam-to-column subassemblies. Both specimens used the ductile connector system: one of them had a T-shaped beam section with concentric prestressing, while the other had the rods only with a rectangular beam section. Subjected to reversed cyclic loading at drift ratios over 7%, both specimens experienced low to intermediate damage around the joint region, but they retained high lateral resistance with adequate damping characteristics.

Due to comprehensive and dedicated efforts encompassing both academia and industry, a variety of precast concrete connection systems have been developed and studied; however, some of the connections, including the welded, hybrid, and prestressing types, may involve complex and heavy on-site workloads. Bolted-type interior connections using ductile rods have shown good seismic performance and can be applied in the field in a simpler fashion, but the exterior version of this connection type has not been experimentally evaluated. This study presents a ductile rod exterior connection specifically developed for applications to precast concrete pipe rack frames in industrial plants. Design and fabrication processes of the exterior connection are first addressed in detail; its seismic performance and important design considerations are then examined through full-scale experimentation.

Development of precast concrete exterior beam-to-column connection

To supplement existing precast concrete connection systems, this study develops a precast concrete exterior beam-to-column connection. The developed moment-resisting exterior connection aims to fully exploit the benefits of the pure dry-cast method, enhance the constructibility of frames with easy joint connection and less congestion, provide better economic feasibility by adopting lower-cost components, and achieve sufficient levels of deformation capability applicable in high seismic regions. **Figure 1** presents components of the exterior beam-to-column connection system, which consists of ductile rods with circular heads embedded in the column, high-strength threaded bars placed along the beam, and a pair of steel transfer blocks with high-tension bolts (ASTM A490[16]) connecting them to the ductile rods.

The bolted connection enables fast and easy assembly of the beam and column components on the construction site and effectively transfers forces between the threaded bars and ductile rods. The ductile rods are designed as the only yielding component, allowing the joint to behave in a ductile manner by forming a plastic hinge within the column. The center region of the ductile rods has a reduced cross-sectional area,

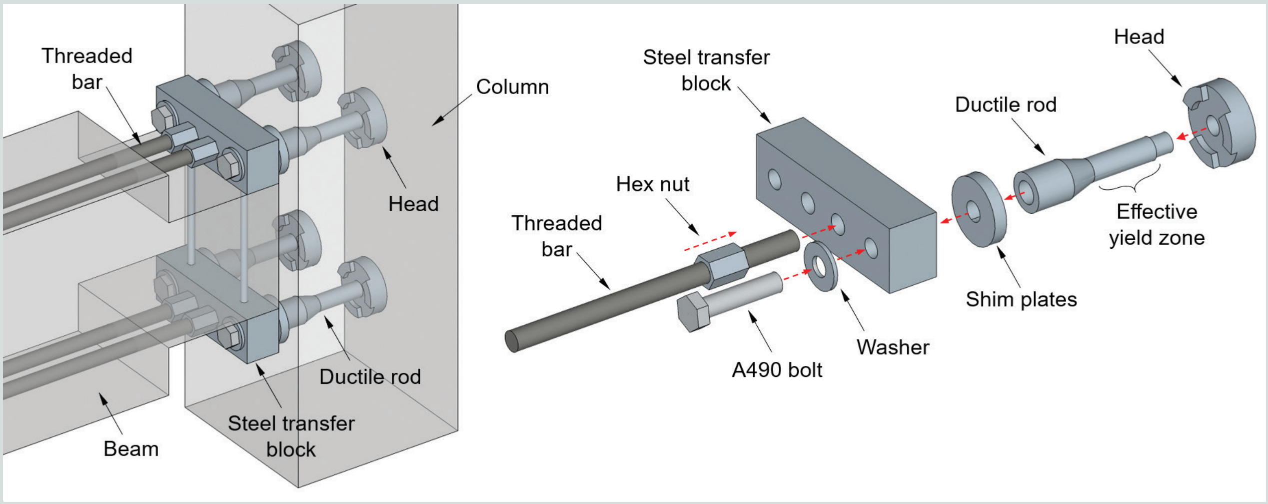

Figure 1. Components and assembly of the precast concrete exterior beam-to-column connection system.

designated as an effective yield zone (Fig. 1). Equations (1) and (2) were used in the design of the threaded bars, A490 bolts, and ductile rods.

$$\phi_1 A_{bolt} F_{nt} \geq A_{rod} f_{y,rod} \quad (1)$$

where

ϕ_1 = resistance factor that conservatively considers uncertainties in load and effective (reduced) tension area of the threaded portion, as specified in American Institute of Steel Construction's (AISC's) *Specification for Structural Steel Buildings*[17] = 0.75

A_{bolt} = cross-sectional area of A490 bolt under combined tension and shear

F_{nt} = nominal tensile strength of the A490 bolt under combined tension and shear

A_{rod} = cross-sectional area of ductile rod

$f_{y,rod}$ = nominal yield strength of ductile rod

$$\phi_2 n_{thr} A_{thr} f_{y,thr} \geq n_{rod} A_{rod} f_{y,rod} \quad (2)$$

where

ϕ_2 = resistance factor for tension yielding in gross section, as specified in AISC specification[17] = 0.9

n_{thr} = number of high-strength threaded bar

A_{thr} = cross-sectional area of high-strength threaded bar

$f_{y,thr}$ = nominal yield strength of high-strength threaded bar

n_{rod} = number of ductile rods

For connection of the ductile rods and transfer block, a tightening torque of 1393 N-m (1027 lb-ft) was applied to the A490 bolts, inducing about 25% of the nominal yield strength of the bolts (Eq. [3]).

$$T = KD_{bolt} N_{bolt} \quad (3)$$

where

T = torque

K = coefficient of torque = 0.15[18]

D_{bolt} = diameter of high-tension bolt

N_{bolt} = tension in bolt induced by tightening = 25% of the yield strength

The adequacy of the ASTM A490 bolts for combined tension and shear at the joint interface was also checked according to the AISC specification[17] and per Englekirk.[19] The uneven surface of the circular head is intended to avoid unwanted spinning of the ductile rod during connection with the transfer block.

Experimental program

In this study, the seismic performance of the developed exterior connection system was experimentally investigated through a series of quasi-static cyclic lateral loading tests. A total of five full-scale precast concrete beam-to-column connection subassemblies representing T-shaped exterior joints were constructed for testing. For the purpose of comparing responses of the precast concrete connections with those of cast-in-place reinforced concrete connections, two comparable full-scale conventional reinforced concrete beam-to-column joint specimens were also constructed and tested under the equivalent lateral loading.

Test specimens

The precast concrete test specimens incorporated various design parameters, such as diameter and development length of the ductile rods, flexural and shear strengths of the beam-to-column connections, and the existence of prestressing steel tendons. **Table 1** summarizes the main properties of all test specimens used in this study. The specimens can be divided into two main configurations depending on the size (cross-sectional area) of the column and beam components.

The column and beam dimensions of the configuration 1 specimens were 500 × 500 mm (19.7 × 19.7 in.) and 400 × 650 mm (15.8 × 25.6 in.), respectively. The PC specimen label indicates precast concrete specimens reinforced with two threaded bars (40 mm [1.57 in.] diameter) and two ductile rods (typically 45 mm [1.8 in.] diameter). One of the precast concrete specimens, PC1-T, was prestressed using three steel tendons (12.7 mm [0.5 in.] diameter) in the beam. Specimen PC1S had two ductile rods of smaller diameter (35 mm [1.4 in.]) to explore the structural response of a connection with reduced flexural strength capacity.

The column and beam dimensions of the configuration 2 specimens were larger: 700 × 700 mm (27.6 × 27.6 in.) and 500 × 700 mm (19.7 × 27.6 in.), respectively. The precast concrete specimens in configuration 2 had three ductile rods (45 mm [1.8 in.] diameter) with a longer development length (400 mm [15.8 in.]) and were labeled according to the same system as the configuration 1 specimens.

Two conventional reinforced concrete specimens (designated C-RC) were constructed according to a strong column–weak beam design concept. One was assigned to each specimen configuration, and these reinforced concrete specimens were designed to have flexural strength capacity comparable to that of their precast concrete specimen counterparts.

Table 1. Details of the test specimens

Configuration	Specimen	Column		Beam		Connection
		Dimensions, mm	Longitudinal reinforcement	Dimension, mm	Longitudinal reinforcement	Ductile rod quantity-diameter length, mm
1	C-RC1	500 × 500	12 D25 bars	400 × 650	Ten D29 bars	n/a (monolithic connection without ductile rods)
	PC1	500 × 500	12 D25 bars	400 × 650	Four D22 bars and four 40 mm diameter threaded bars	Two 45 × 300
	PC1-T	500 × 500	12 D25 bars	400 × 650	Four D22 bars, four 40 mm diameter threaded bars, and three 12.7 mm diameter prestressing tendons	Two 45 × 300
	PC1S	500 × 500	12 D25 bars	400 × 650	Four D22 bars and four 36 mm diameter threaded bars	Two 35 × 300
2	C-RC2	700 × 700	12 D29 bars	500 × 700	Sixteen D29 bars	n/a (monolithic connection without ductile rods)
	PC2	700 × 700	12 D29 bars	500 × 700	Six D25 bars and four 40 mm diameter threaded bars	Three 45 × 400
	PC2-T	700 × 700	12 D29 bars	500 × 700	Six D25 bars, four 40 mm diameter threaded bars, and three 12.7 mm diameter prestressing tendons	Three 45 × 40

Note: Configuration 1 specimens have a 500 × 500 mm column and 400 × 650 mm beam configuration, and configuration 2 specimens have a 700 × 700 mm column and 500 × 700 mm beam configuration. C-RC1 = conventional reinforced concrete specimen with configuration 1 dimensions; C-RC2 = conventional reinforced concrete specimen with configuration 2 dimensions; n/a = not applicable; PC1 = precast concrete specimen with configuration 1 dimensions; PC1S = precast concrete specimen with smaller diameter ductile rods and configuration 1 dimensions; PC1-T = precast concrete specimen with prestressed tendons and configuration 1 dimensions; PC2 = precast concrete specimen with configuration 2 dimensions; PC2-T = precast concrete specimen with prestressed tendons and configuration 2 dimensions. 1 mm = 0.0394 in.

Figures 2 and **3** show the cross sections and configurations of the beam-to-column connection subassemblies, as well as details of the connection components used in this study. **Table 2** provides the design strength of each beam-to-column joint specimen. The nominal moment strength M_n of the precast concrete specimens was assumed to be governed by yielding of the ductile rods and was calculated using Eq. (4), based on the American Concrete Institute's (ACI's) *Building Code Requirements for Structural Concrete (ACI 318-19) and Commentary (ACI 318R-19)*.[20]

$$M_n = n_{rod} A_{rod} f_{y,rod} (d_{rod} - d'_{rod}) \tag{4}$$

where

d_{rod} = distance from beam's top face to centroid of bottom ductile rod

d'_{rod} = distance from beam's top face to centroid of top ductile rod

The nominal shear strength V_n and shear force demand on the joint V_j of the precast concrete specimens were calculated using Eq. (5) and (6), respectively, following ACI 352R-02.[21] Note that PC1-T and PC2-T were expected to have unbalanced positive and negative strengths because of the eccentrically provided prestressing tendons.

$$V_n = 0.083\gamma\sqrt{f'_c}A_j \tag{5}$$

where

f'_c = nominal compressive strength of concrete

γ = coefficient for the connection type = 12

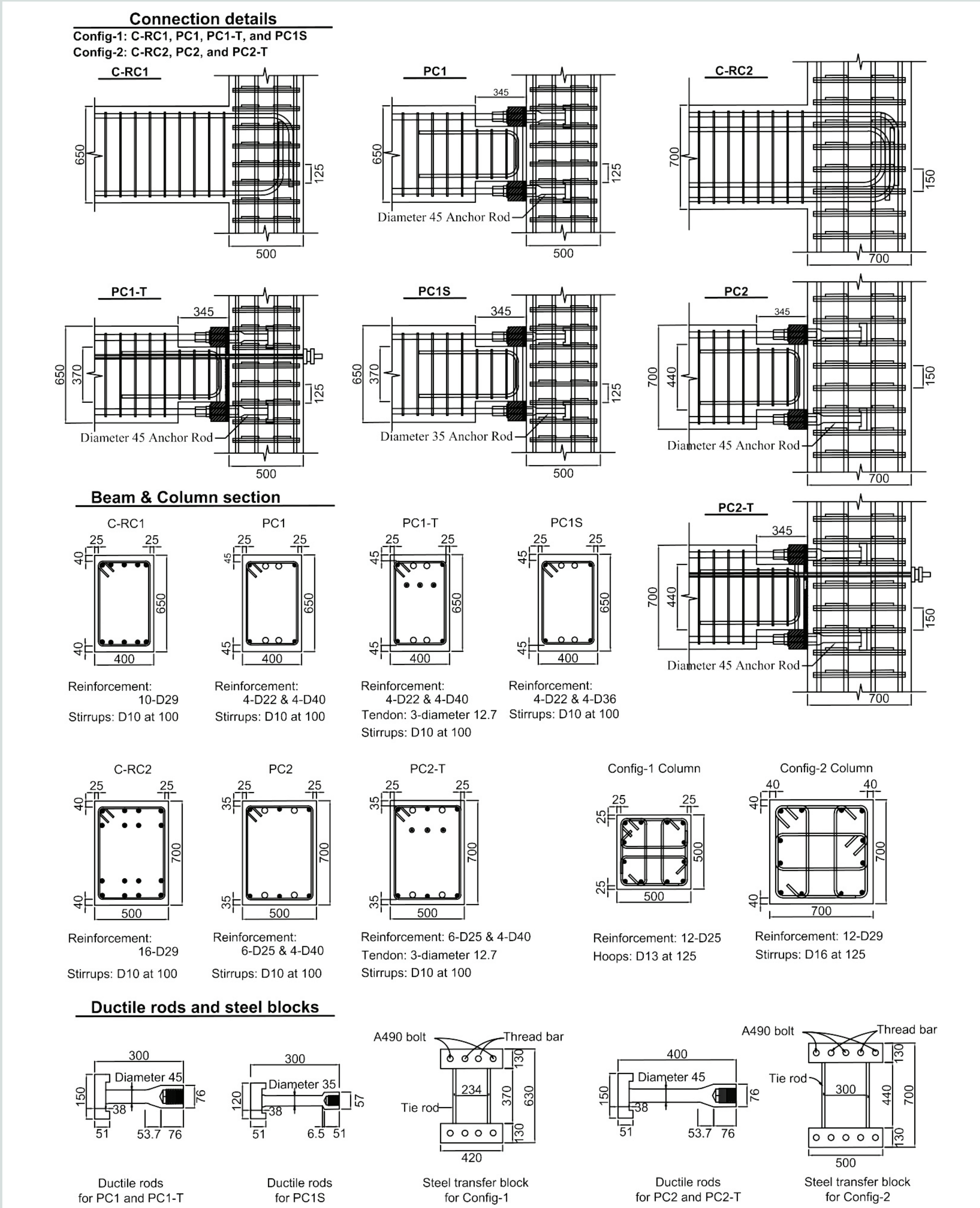

Figure 2. Configuration and details of the beam-to-column subassemblies. Note: All dimensions in millimeters. Config-1 = specimen with 500 × 500 mm column and 400 × 650 mm beam configuration; Config-2 = specimen with 700 × 700 mm column and 500 × 700 mm beam configuration; C-RC1 = conventional reinforced concrete specimen with configuration 1 dimensions; C-RC2 = conventional reinforced concrete specimen with Config-2 dimensions; PC1 = precast concrete specimen with Config-1 dimensions; PC1S = precast concrete specimen with smaller diameter ductile rods and Config-1 dimensions; PC1-T = precast concrete specimen with prestressed tendons and Config-1 dimensions; PC2 = precast concrete specimen with Config-2 dimensions; PC2-T = precast concrete specimen with prestressed tendons and Config-2 dimensions. 1 mm = 0.0394 in.

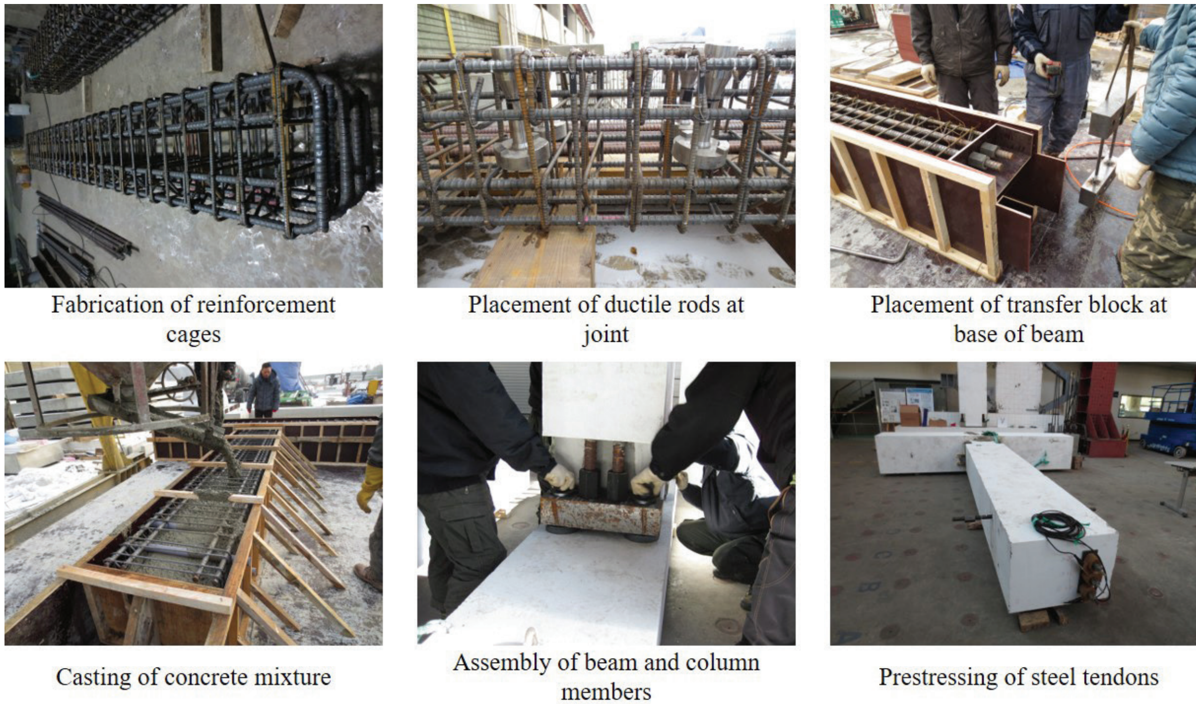

Figure 3. Construction process of the precast concrete exterior beam-to-column connection specimens.

Table 2. Calculation of nominal moment capacity and shear forces and strengths at the joint

Configuration	Specimen	Nominal moment capacity M_n, kN-m	Joint shear force V_j, kN	Nominal shear strength V_n,* kN	V_j/V_n
1	C-RC1	683	1341	1331	1.01
	PC1	660	1414	1331	1.06
	PC1-T	+778/-686	+1512/−1374	1331	1.14/1.03
	PC1S	400	856	1331	0.64
2	C-RC2	1063	2067	2485	0.83
	PC2	1128	2071	2485	0.83
	PC2-T	+1227/-1125	+2123/−1999	2485	0.86/0.8

Note: Configuration 1 specimens have a 500 × 500 mm column and 400 × 650 mm beam configuration, and configuration 2 specimens have a 700 × 700 mm column and 500 × 700 mm beam configuration. ACI = American Concrete Institute; configuration 1 = specimens with 500 × 500 mm column and 400 × 650 mm beam configuration; configuration 2 = specimens with 700 × 700 mm column and 500 × 700 mm beam configuration; C-RC1 = conventional reinforced concrete specimen with configuration 1 dimensions; C-RC2 = conventional reinforced concrete specimen with configuration 2 dimensions; PC1 = precast concrete specimen with configuration 1 dimensions; PC1S = precast concrete specimen with smaller diameter ductile rods and configuration 1 dimensions; PC1-T = precast concrete specimen with prestressed tendons and configuration 1 dimensions; PC2 = precast concrete specimen with configuration 2 dimensions; PC2-T = precast concrete specimen with prestressed tendons and configuration 2 dimensions. 1 mm = 0.0394 in.; 1 kN = 0.225 kip; 1 kN-m = 0.738 kip-ft.

* According to ACI 352R-02.

A_j = effective joint area

$$V_j = n_{rod}A_{rod}\alpha f_{y,rod} - \alpha M_n/h_c \quad (6)$$

where

α = stress multiplier for longitudinal reinforcement to account for its actual yield stress = 1.25

h_c = distance between column supports in the test setup

Different joint shear demand-to-capacity ratios V_j/V_n were applied to verify the behavior of individual components as well as resistance and damage mechanisms in the connection systems. While the configuration 2 specimens (C-RC2, PC2, and PC2-T) were designed to have sufficient joint shear capacity, with V_j/V_n close to 0.8, the typical configuration 1 specimens (C-RC1, PC1, and PC1-T) had V_j/V_n close to or even greater than 1. (PC1S was designed with sufficient joint shear capacity due to its reduced flexural strength capacity.) Table 2 presents the expected shear demand-to-capacity ratio for each specimen.

Unlike the reinforced concrete specimens that had a monolithic connection, each beam and column pair for the precast concrete specimens was cast separately on the same day and then assembled after curing. Figure 3 shows the construction process of the precast concrete specimens, including fabrication of reinforcement cages, placement of the ductile rods and steel block, casting of the concrete, and assembly of the beam and column. For PC1-T and PC2-T, the steel tendons penetrating the specimen were prestressed after the components were assembled, with the interface of the beam and column first filled with grouting material for effective transfer of the compression force generated by the prestressing.

Material properties

Concrete with a target compressive strength of 35 MPa (5.1 ksi) and steel reinforcing bars with a minimum (nominal) yield strength of 400 MPa (58 ksi) were used to construct the test specimens. **Table 3** gives the compressive strength of concrete f'_c measured on the day of subassembly testing. It also shows experimentally obtained yield strength f_y, measured yielding stress of stirrups $f_{y,h}$, measured yielding stress of ductile rods $f_{y,rod}$, and measured yielding stress of threaded bars $f_{y,thr}$ values for the longitudinal steel bars, transverse stirrups, ductile rods, and high-strength threaded bars, respectively. The yield strengths of D29 reinforcing bars (with a yield strength f_y of 536.5 MPa [77.8 ksi]) and D22 reinforcing bars (with a yield strength f_y of 554.8 MPa [80.5 ksi]) used in the configuration 1 specimens and C-RC2 (Table 1) turned out to be much higher than their nominal yield strength. The steel tendons used in specimens PC1-T and PC2-T exhibited an average ultimate tensile strength $f_{u,ten}$ of 1893 MPa (274.6 ksi). Two months before testing, the tendons in those specimens were prestressed with a prestressing force reaching 85% of their tensile strength, but some prestressing force was lost due to shrinkage and creep (including gradual elastic shortening) of the concrete. Table 3 gives the average effective prestressing value $f_{eff,ten}$ at subassembly testing.

Table 3. Properties of materials used in beam components

Configuration	Specimen	Measured compressive strength of concrete f'_c, MPa	Measured yielding stress of reinforcing bars f_y, MPa	Measured yielding stress of stirrups $f_{y,h}$, MPa	Measured yielding stress of threaded bars $f_{y,thr}$, MPa	Measured yielding stress of ductile rods $f_{y,rod}$, MPa	Ultimate stress of tendons $f_{u,ten}$, MPa	Effective prestress of tendons $f_{eff,ten}$,* MPa
1	C-RC1	38.3	536.5	487.7	n/a	n/a	n/a	n/a
	PC1	38.5	554.8	487.7	1001	413.7	n/a	n/a
	PC1-T	36.9	554.8	487.7	1001	413.7	1893	773
	PC1S	42.5	554.8	487.7	1001	413.7	n/a	n/a
2	C-RC2	43.6	536.5	487.7	n/a	n/a	n/a	n/a
	PC2	43.6	484.3	487.7	1001	413.7	n/a	n/a
	PC2-T	54.1	484.3	487.7	1001	413.7	1893	778.1

Note: Configuration 1 specimens have a 500 × 500 mm column and 400 × 650 mm beam configuration, and configuration 2 specimens have a 700 × 700 mm column and 500 × 700 mm beam configuration. C-RC1 = conventional reinforced concrete specimen with configuration 1 dimensions; C-RC2 = conventional reinforced concrete specimen with configuration 2 dimensions; n/a = not applicable. PC1 = precast concrete specimen with configuration 1 dimensions; PC1S = precast concrete specimen with smaller diameter ductile rods and configuration 1 dimensions; PC1-T = precast concrete specimen with prestressed tendons and configuration 1 dimensions; PC2 = precast concrete specimen with configuration 2 dimensions; PC2-T = precast concrete specimen with prestressed tendons and configuration 2 dimensions. 1 mm = 0.0394 in.; 1 MPa = 0.145 ksi.

* Measured on the day of testing.

Testing

Figure 4 depicts the test setup used to simulate seismic loading conditions for the T-shaped beam-to-column connection subassemblies. In this test setup, the column was placed horizontally with pinned supports at both ends, assuming that each end represents an inflection point that has zero bending moment. For application of cyclic lateral loading, an actuator with force capacity up to +900/–550 kN (+202/–124 kip) was installed at the top of the beam. Out-of-plane deflection of the specimens was prevented by installing steel ball jigs at f_y the midpoint of the beam on both sides. The vertical distance from the face of the column to the center of the loading point for the configuration 1 and configuration 2 specimens was 3800 and 3600 mm (150 and 142 in.), respectively. Figure 4 further illustrates the loading protocol, determined in accordance with ACI 374.1-05.[22] The actuator applied displacement-controlled lateral loading to the top of the beam at a rate of approximately 0.3 to 1.5 mm/sec (0.012 to 0.059 in./sec) in both the positive and negative directions. The actuator initially imposed low-level displacements, corresponding to an interstory drift ratio of 0.5% and then incrementally increased to a 5% drift ratio. Three cycles of loading were repeated at each target drift. The specimens were considered to reach their ultimate state if they experienced a significant strength degradation. Therefore, testing was typically terminated when the lateral force dropped below 80% of the peak measured force. During testing, no axial force was applied to the column. This was intended to conservatively evaluate the connection performance without any axial confinement of the joint region.

A certain level of compressive force in the column (less than approximately 30% of its axial capacity) can be effective in enhancing joint behavior by securing the ductile rods and delaying concrete cracking.

Figure 4 also shows different types of sensors installed to capture the global and local structural responses of the specimens. Lateral displacement of the beam was measured by one linear variable displacement transducer (LVDT) internally installed in the actuator and one cable extension transducer installed at the midpoint of the beam. Four LVDTs were used to measure flexural deformation of the beam and slippage of the reinforcement near the interface of the beam and column. Shear distortion of the beam-to-column joint was measured by two pairs of LVDTs attached on the front and back sides of the joint, respectively. Four LVDTs were also placed to check if there was any vertical or horizontal slippage of the specimens at the pinned supports. The lateral resistance force of the specimens was measured by a load cell installed in the actuator. For the specimens with prestressing tendons (PC1-T and PC2-T), six additional load cells were used to monitor the prestressing force of the steel tendons. Strain gauges were also used to measure local deformations of the steel reinforcing bars, ductile rods, and threaded bars.

Test observations and results

Overall behavior

All configuration 1 specimens sustained their cyclic lateral loading up to 5% drift ratio, except for PC1S. As a result of

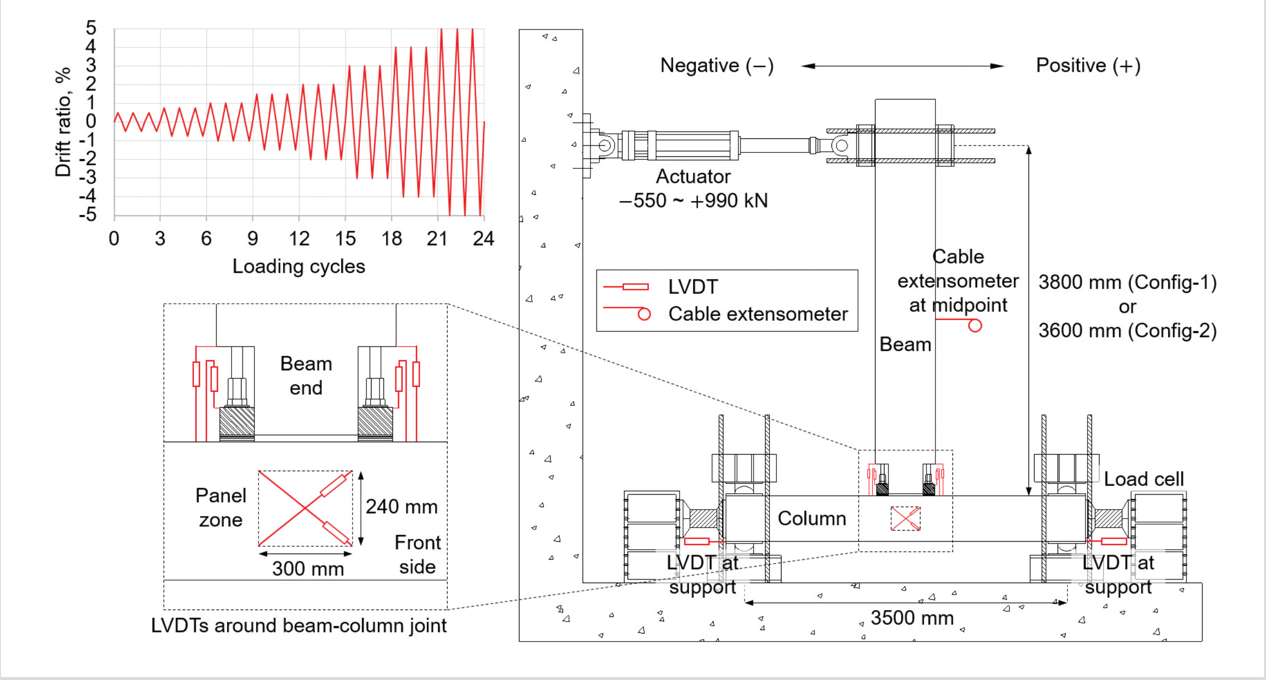

Figure 4. Test setup and loading protocol. Note: Config-1 = specimens with 500 × 500 mm column and 400 × 650 mm beam configuration; Config-2 = specimens with 700 × 700 mm column and 500 × 700 mm beam configuration; LVDT = linear variable displacement transducer. 1 mm = 0.0394 in.; 1 kN = 0.225 kip.

insufficient joint shear capacity ($V_j/V_n \approx 1$), most damage appeared in the joint region of the columns, with critical concrete cracking eventually contributing to failure of the specimens. **Figure 5** shows the final damage status of the configuration 1 specimens.

In the specimen with a monolithic connection, C-RC1, initial damage appeared as minor flexural and shear cracks in the beam and joint during early stages of loading. Under higher drift ratios (above 4%), the joint shear cracking developed as large, symmetric X-shaped diagonal cracks, extending over the entire joint region. C-RC1 experienced severe spalling of cover concrete on both sides of the joint.

Specimens PC1 and PC1-T showed quite similar damage propagation. At a drift ratio of 0.5%, horizontal concrete cracking was initially observed at the beam base along the embedded tie rod (Fig. 2) of the transfer blocks. When subjected to drift ratios beyond 2%, both specimens began to develop diagonal cracks in the upper-half region of the joint. These cracks grew and widened, developing a W-shaped cracking zone in the joint of each column. At ±5% drift ratios, both precast concrete specimens lost large chunks of cover concrete.

The different joint failure patterns of the reinforced concrete and precast concrete specimens can be explained by their different resistance mechanisms. In C-RC1, because the beam's longitudinal bars extended and were hooked near the exterior column surface (Fig. 2), the entire joint was engaged in the cyclic shearing actions transferred from the beam. On the other hand, joints of the precast concrete specimens were strongly governed by push-in and pullout actions of the ductile rods anchored at mid-depth of the columns. The upper joint region was partially involved when the ductile rods were pulled out, forming the W-shaped crack pattern. Due to the cracking, subsequent spalling of cover concrete eventually occurred in both PC1 and PC1-T (Fig. 5).

The testing of PC1S was terminated prematurely, during the first cycle of 1.5% drift ratio, because of an unexpected rup-

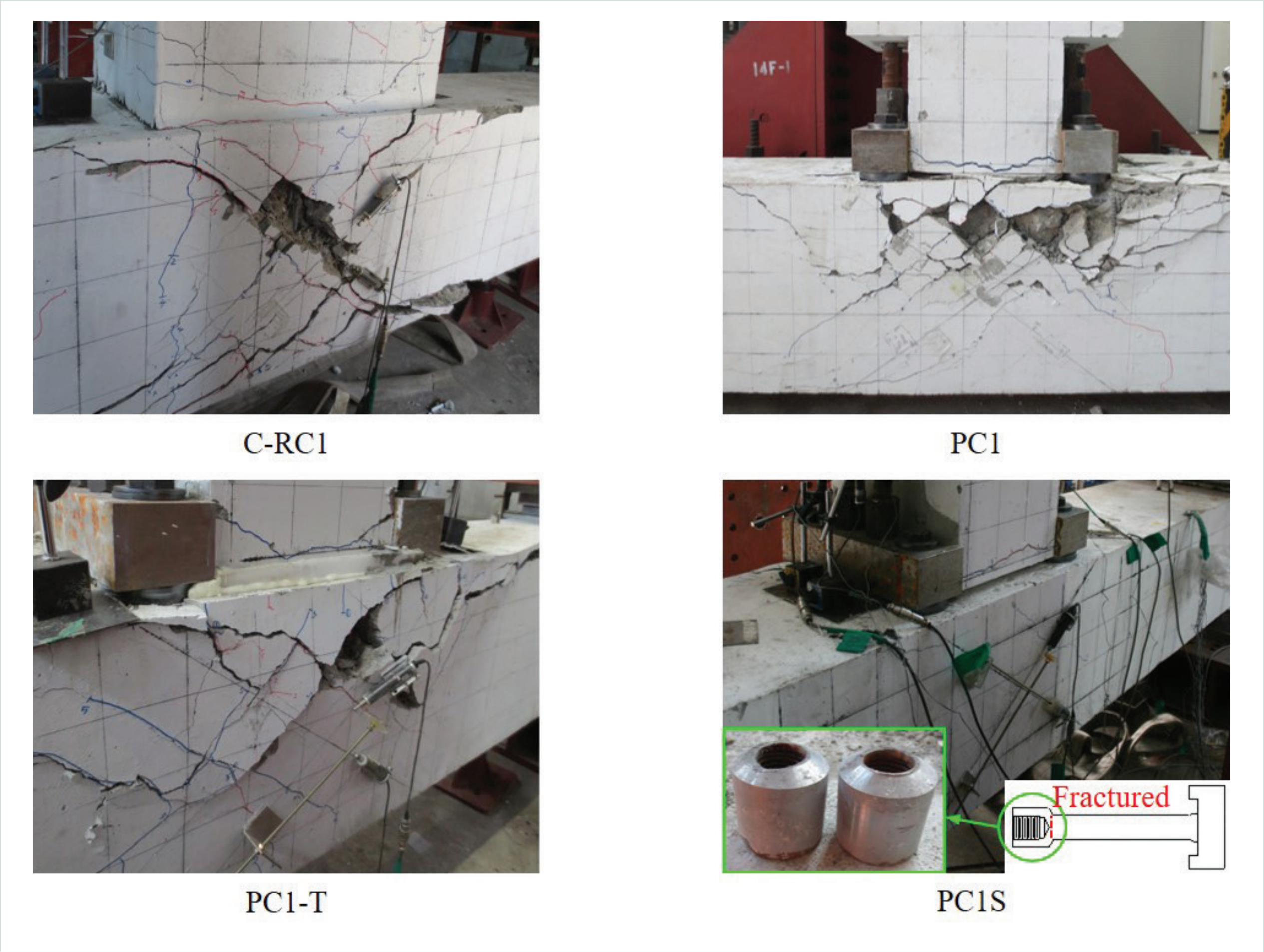

Figure 5. Final damage status of Config-1 specimens. Note: Config-1 = specimens with 500 × 500 mm column and 400 × 650 mm beam configuration; C-RC1 = conventional reinforced concrete specimen with Config-1 dimensions; PC1 = precast concrete specimen with Config-1 dimensions; PC1S = precast concrete specimen with smaller diameter ductile rods and Config-1 dimensions; PC1-T = precast concrete specimen with prestressed tendons and Config-1 dimensions. 1 mm = 0.0394 in.

ture of the ductile rods (Fig. 5). All ductile rods had a hollow space with a threaded inner surface for connection with the A490 bolts (Fig. 2). The hollow space of the ductile rods in PC1S approached the effective yield zone too closely. This design flaw sharply decreased the effective cross-sectional area, creating a point in the ductile rods that was too weak to transfer the force of the longitudinal bars.

Configuration 2 specimens were subjected to cyclic lateral loading up to 4% to 5% drift ratios but exhibited different damage and failure patterns than those of the configuration 1 specimens. Due to the increased column size and sufficient joint shear capacity ($V_j/V_n \approx 0.8$), the joints of configuration 2 specimens were not heavily damaged. **Figure 6** shows the final damage status of the configuration 2 specimens. In C-RC2, horizontal flexural cracks appeared around the base of the beam at 1% drift ratio and were soon followed by minor shear cracks in the joint. At drift ratios of approximately 4% to 5%, the beam's flexural cracks developed more prominently, contributing to the formation of a complete plastic hinge that involved severe spalling of cover concrete and buckling of reinforcing bars.

Similar to the configuration 1 precast concrete specimens, PC2 experienced initial horizontal cracking along the tie rod at 0.5% drift ratio and several vertical cracks were found near the base of the beam. As the drift ratios further increased, more vertical cracks formed along and adjacent to the threaded bars toward the top of the beam, which eventually led to splitting of concrete and bond failure of the threaded bars in the first cycle to ±4% drift ratio. In PC2, the number of ductile rods increased to three, but the number of threaded bars remained the same. Accordingly, higher flexural demands and bond stresses were imposed on the threaded bars than for PC1. It seemed that due to the high bond stresses, the concrete split (Fig. 6) when the ribs of the threaded bars (40 mm [1.6 in.] diameter) were bearing against the surrounding concrete (wedging action). Such bond failure should be preventable simply by providing sufficient development length for the threaded bars.

The damage pattern of PC2-T was quite similar to that of PC2, as vertical cracks developed on the top and bottom beam surfaces and then resulted in bond failure along the threaded bars. However, its damage propagation occurred much later than that of PC2 and it successfully completed the full cycles of ±4% drift ratio. The prestressing tendons shared the flexural demand imposed on the beam, alleviating the forces acting in the threaded bars. Both PC2 and PC2-T showed minor diagonal joint cracks.

Flexural response

Figures 7 and **8** present the flexural responses of the configuration 1 and configuration 2 specimens, respectively, in terms of moment-to-drift ratio relationships. Beam end moment was calculated as the actuator force times the vertical distance between the beam-to-column interface and the loading point (Fig. 4). Drift ratio was calculated as the beam's lateral displacement divided by the vertical distance between the column centerline and the loading point.

Table 4 summarizes the main response parameters. Figures 7 and 8 present the expected flexural capacities of the specimens M_{exp}, which were recalculated based on the measured material strengths (Table 3). The measured peak moment M_{pk}

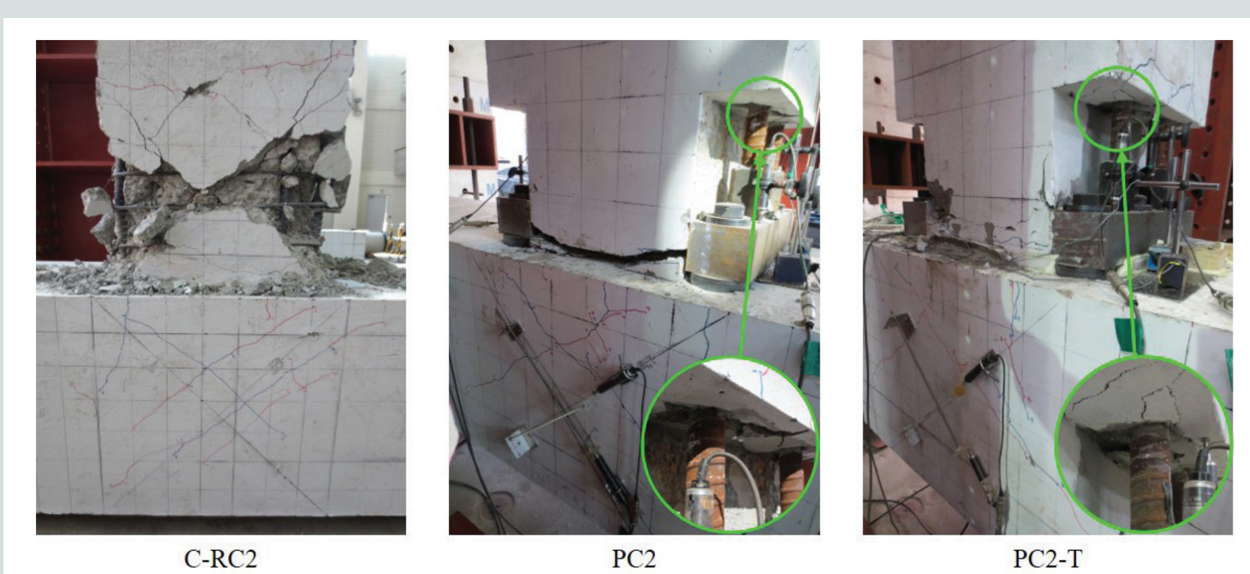

Figure 6. Final damage status of configuration 2 specimens. Note: Config-2 = specimens with 700 × 700 mm column and 500 × 700 mm beam configuration; PC2 = precast concrete specimen with Config-2 dimensions; PC2-T = precast concrete specimen with prestressed tendons and Config-2 dimensions. 1 mm = 0.0394 in.

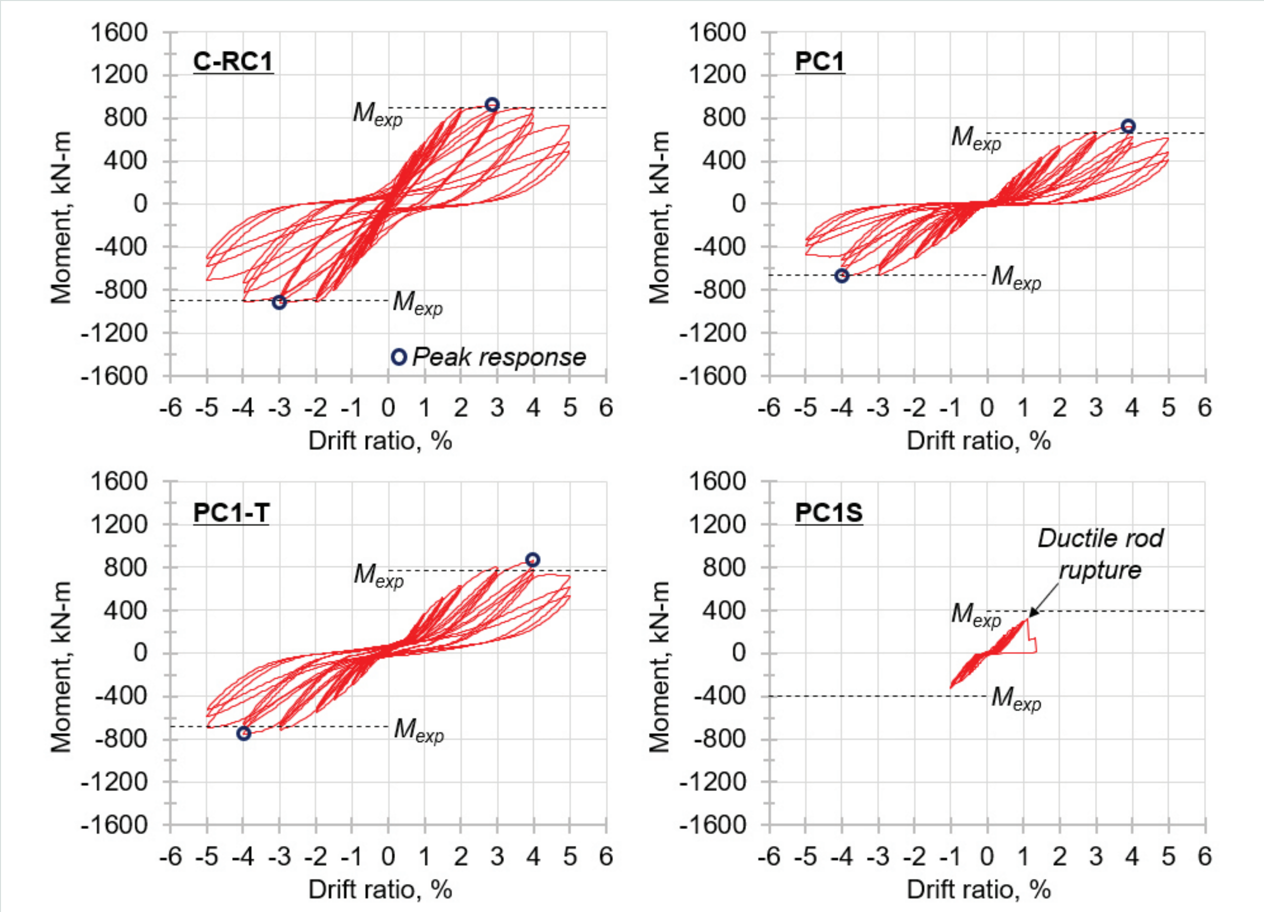

Figure 7. Moment-to-drift ratio relationships of the configuration 1 specimens. Note: Config-1 = specimens with 500 × 500 mm column and 400 × 650 mm beam configuration; C-RC1 = conventional reinforced concrete specimen with Config-1 dimensions; M_{exp} = expected moment strength based on measured material properties; PC1 = precast concrete specimen with Config-1 dimensions; PC1S = precast concrete specimen with smaller diameter ductile rods and Config-1 dimensions; PC1-T = precast concrete specimen with prestressed tendons and Config-1 dimensions. 1 mm = 0.0394 in.; 1 kN-m = 0.738 kip-ft.

values matched M_{exp} well, except for PC1S. The drift ratio at yield d_y was estimated based on recommendations from ACI 374.2R-13.[23] The ultimate drift ratio d_u was determined when the measured moment dropped below 80% of M_{pk} in the first loading cycle or when a significant moment reduction occurred in any loading cycle.

The configuration 1 specimens exhibited overall stable responses (Fig. 7) except for PC1S, which suffered brittle failure of the ductile rods. C-RC1 demonstrated the greatest flexural capacity among all configuration 1 specimens. The considerable moment of C-RC1 resulted from the unexpectedly high yield strength of the D29 bars (Table 3). During drift ratios of between approximately 2% and 4%, C-RC1 retained high flexural resistance of about 900 kN-m (663.8 kip-ft), recording peak moments in cycles of ±3% drift ratio. The moment of C-RC1 dropped below 80% of its peak at a drift ratio of -4.84%, with a corresponding displacement ductility μ_d of 2.95. In the case of PC1, yielding occurred at drift ratios of +2.6% and -2.72%, and the peak moments (of +713.3 kN-m [+516.1 kip-ft] and -677.8 kN-m [-499.9 kip-ft]) achieved the expected flexural capacity at +3.91% and –4%, respectively. Despite severe joint damage (Fig. 5), PC1 demonstrated its lateral deformation capacity up to ±5% drift ratio without significant strength reduction. The peak responses of PC1 were exhibited about 1% later than for C-RC1. This was primarily due to the overall lower lateral stiffness of PC1. Furthermore, PC1 exhibited significantly reduced stiffness near the origin during load reversals (Fig. 7). It is presumed that this pinching behavior, which contrasts clearly with the behavior of the monolithic connection, occurred due to gap opening at the interface of the bolted connection. PC1-T showed quite similar response to that of PC1. PC1-T recorded its peak moment during ±4% loading cycles, with an obvious pinching effect. The prestressing tendons that were eccentrically added to the beam increased the flexural capacity of PC1-T in the positive direction, resulting in 14.2% higher peak moment than that in the negative direction (Table 4). PC1-T successfully sustained the full loading cycles and maintained its flexural resistance above 80% of the peak moment in both directions. PC1S mostly showed elastic response and then suddenly failed due

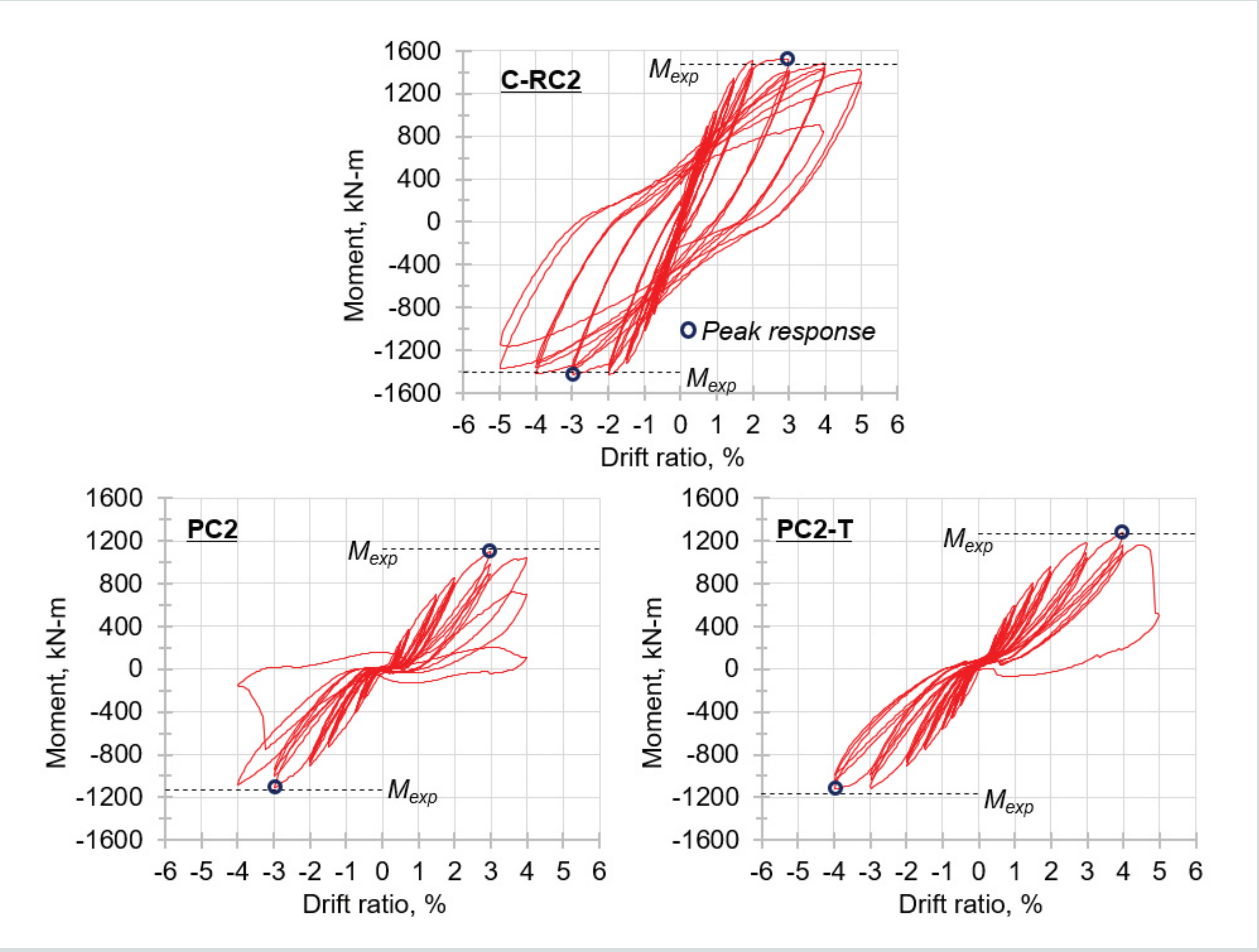

Figure 8. Moment-drift ratio relationships of the configuration 2 specimens. Note: Config-2 = specimens with 700 × 700 mm column and 500 × 700 mm beam configuration; C-RC2 = conventional reinforced concrete specimen with Config-2 dimensions; M_{exp} = expected moment strength based on measured material properties; PC2 = precast concrete specimen with Config-2 dimensions; PC2-T = precast concrete specimen with prestressed tendons and Config-2 dimensions. 1 mm = 0.0394 in.; 1 kN-m = 0.738 kip-ft.

to rupture of the ductile rods at a drift ratio of +1.1%; only 80% of the expected flexural capacity was achieved by PC1S.

Among the configuration 2 specimens, C-RC2 showed very high flexural capacity due to the high yield strength of the D29 bars (Table 3). High moment, exceeding 1400 kN-m (1032.6 kip-ft), was maintained until the first cycle of 5% drift. In the third cycle, however, C-RC2 was no longer able to carry the load because of the buckling of longitudinal bars, with recorded displacement ductility μ_d greater than 3. PC2 exhibited well-balanced flexural capacity in both directions, with peak moments of about 1100 kN-m (811.3 kip-ft) at ±3% drift ratio. The lateral resistance of PC2 dramatically deteriorated during the 4% drift loading cycles after the onset of bond failure of the threaded bars (Fig. 6), and it ended up with an average displacement ductility μ_d of about 1.63. The response of PC2 was also clearly affected by similar pinching behavior observed in the configuration 1 precast concrete specimens. Specimen PC2-T, equipped with the prestressing tendons, exhibited peak moments at ±4% drift ratio, which is 1% drift later than PC2. About 13.3% greater peak moment was obtained in the positive direction with the aid of the added steel tendons. Unlike PC2, PC2-T was able to complete the full loading cycles up to 4% drift without losing its lateral load resistance and then failed in the subsequent 5% drift loading cycle. Although more in-depth study is needed on the effect of prestressing, this experimental result indicates that it played a role in delaying damage propagation and increasing the flexural strength of the precast concrete beam-to-column connections.

Joint shear response

Figure 9 illustrates the shear responses of the joint panels up to 4% drift ratio through shear force-distortion relationships. The joint shear forces are normalized by the expected shear capacities V_{exp}, which were recalculated based on the measured material strengths (Table 3). (The response of PC1S, which showed premature ductile rod failure, is not reported.) Figure 9 also shows the peak responses corresponding to the first cycles of 3% and 4% drift ratios.

Table 4. Summary of test results

Configuration	Specimen	Direction	Measured peak moment M_{pk}, kN-m	M_{pk}/ M_{exp}	Measured peak shear strength of joint $V_{j,pk}$,* kN	$V_{j,pk}$/ V_{exp}	Drift ratio at yielding point d_y,† %	Drift ratio at peak moment d_{pk}, %	Drift at ultimate state d_u, %	Displacement ductility μ_d (d_u/d_y)
1	C-RC1	+	918.2	1.03	1480	1.06	1.71	2.88	n/a	n/a
		–	925.2	1.03	1491	1.07	1.64	2.99	4.84	2.95
	PC1	+	713.3	1.08	1223	0.88	2.6	3.91	n/a	n/a
		–	677.8	1.03	1162	0.83	2.72	4	4.63	1.7
	PC1-T	+	859.3	1.12	1415	1.04	2.84	3.92	n/a	n/a
		–	752.4	1.09	1239	0.90	2.77	3.96	n/a	n/a
	PC1S	+	319.8	0.8	619.3	0.42	n/a	1.1	1.1	n/a
		–	317.9	0.8	615.6	0.42	n/a	1	n/a	n/a
2	C-RC2	+	1525	1.08	2456	0.89	1.52	2.92	4.96	3.26
		–	1428.1	1.01	2300	0.83	1.44	2.97	4.98	3.46
	PC2	+	1100.1	0.98	1830	0.66	2.52	2.97	4	1.59
		–	1102.6	0.98	1834.3	0.66	2.40	2.96	4	1.67
	PC2-T	+	1273.3	1	1864.8	0.6	2.63	3.98	4.77	1.81
		–	1123.7	0.96	1645.2	0.53	2.41	3.95	n/a	n/a

Note: Configuration 1 specimens have a 500 × 500 mm column and 400 × 650 mm beam configuration, and configuration 2 specimens have a 700 × 700 mm column and 500 × 700 mm beam configuration. ACI = American Concrete Institute; C-RC1 = conventional reinforced concrete specimen with configuration 1 dimensions; C-RC2 = conventional reinforced concrete specimen with configuration 2 dimensions; d_u = ultimate drift ratio; M_{exp} = expected moment strength based on measured material properties; n/a = not applicable; PC1 = precast concrete specimen with configuration 1 dimensions; PC1S = precast concrete specimen with smaller diameter ductile rods and configuration 1 dimensions; PC1-T = precast concrete specimen with prestressed tendons and configuration 1 dimensions; PC2 = precast concrete specimen with configuration 2 dimensions; PC2-T = precast concrete specimen with prestressed tendons and configuration 2 dimensions; Vexp = expected shear strength at joint with measured material properties based on ACI 352R-02. 1 mm = 0.0394 in.; 1 kN = 0.225 kip; 1 kN-m = 0.738 kip-ft.

* $V_{j,pk} = M_{pk}/(0.9d) - V_{col}$, where d is effective beam depth and V_{col} is column shear.

† Estimated based on ACI 374.2R-13.

In C-RC1, which exhibited large X-shaped cracks, the shear force at the joint reached its capacity with distortions up to 0.011 rad at 4% drift ratio. Joint shear distortions of approximately 0.01 rad typically have been associated with reaching a reinforced concrete joint's shear strength in well-detailed structural concrete exterior connections.[24] On the other hand, PC1 recorded a normalized joint shear slightly above 0.8 but the maximum joint distortions were higher than 0.015 rad in both directions. Even though PC1 still had a shear force safety margin of more than 10% against joint shear failure, the joint was substantially governed by pullout of the ductile rods and much higher resultant distortions occurred than for C-RC1. The overall hysteretic response of PC1-T was similar to that of PC1, but the range of joint distortion was below ±0.015 rad. Furthermore, PC1-T obtained higher normalized joint shear (greater than 1), especially in the positive direction, indicating that the prestressing tendons acted to increase shear force demand and capacity of the beam-to-column joint.

The normalized joint shear forces and distortions of the configuration 2 specimens were much lower than those of the configuration 1 specimens. This reduced joint shear response agreed with the limited joint damage of the configuration 2 specimens (Fig. 6) and their sufficient joint shear capacity ($V_j/V_n \approx 0.8$) considered in design. The maximum distortion of all configuration 2 specimens was below 0.006 rad, with joint shear force capacity not reached in any configuration 2 specimens (Fig. 9 and Table 4). Furthermore, as the drift ratio changed from ±3% to ±4%, the configuration 2 specimens experienced only small increases in peak distortion of about 0.02 ~ 0.14 × 10^{-2} rad. This increment range was substantially less than the corresponding range for the configuration 1 specimens (0.32 ~ 1.04 × 10^{-2} rad) that experienced critical damage propagation at the joint.

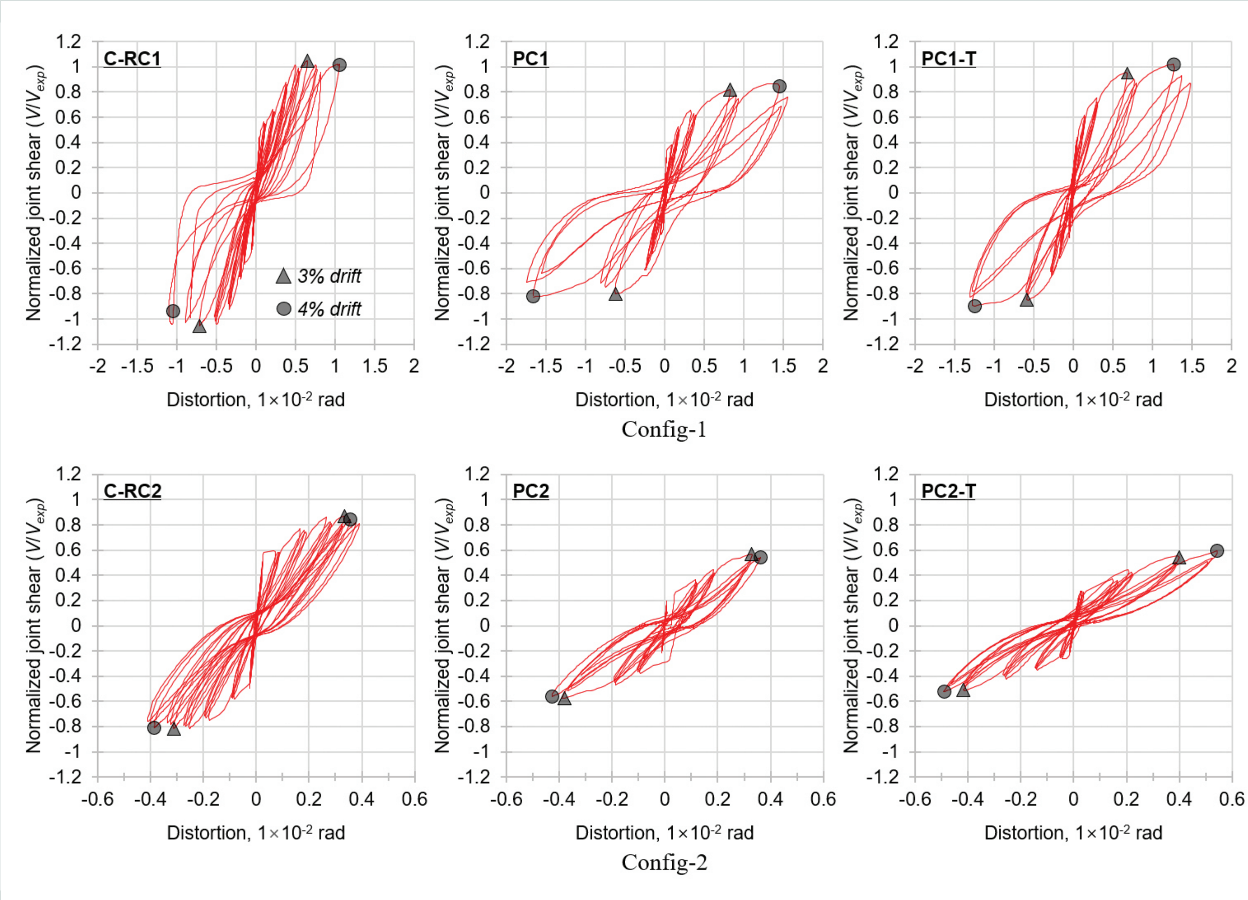

Figure 9. Shear-distortion responses of the joint panels. Note: Config-1 = specimens with 500 × 500 mm column and 400 × 650 mm beam configuration; Config-2 = specimens with 700 × 700 mm column and 500 × 700 mm beam configuration; C-RC1 = conventional reinforced concrete specimen with Config-1 dimensions; C-RC2 = conventional reinforced concrete specimen with Config-2 dimensions; PC1 = precast concrete specimen with Config-1 dimensions; PC1-T = precast concrete specimen with prestressed tendons and Config-1 dimensions; PC2 = precast concrete specimen with Config-2 dimensions; PC2-T = precast concrete specimen with prestressed tendons and Config-2 dimensions; V = joint shear force ; Vexp = expected shear strength at joint with measured material properties. 1 mm = 0.0394 in.

Contribution of flexural and shear deformations at the joint to total drift

To better understand the effects of flexural and shear deformations at the joint region on overall deformation of the specimens, contributions from beam end rotation and joint distortion to the total displacement of each beam were investigated. **Figure 10** shows the contributions of deformation components at each positive target drift, which were estimated based on LVDT measurements around the joint region (Fig. 4).

In C-RC1, the contribution of beam end rotation was maintained at about 30% until reaching 2% drift; it then increased to above 50% by 3% drift. The contribution of joint distortion increased to above 20% relatively early (by 1% drift ratio) and then continued to the end of testing. The rest of the contribution not presented in Fig. 10 is considered mostly attributable to distributed flexural deformation of the beam above the joint region. PC1 and PC1-T showed comparable contribution patterns in which more than 70% of the total displacement in the initial loading stage was from deformations due to beam end rotation. This substantial contribution indicates that deformation of the precast concrete specimens was predominantly concentrated at the beam end due to joint opening. Similar levels of so-called rigid-body rocking end rotation have also been reported in other types of precast concrete structural connections.[25] As the specimens displaced to 4% drift, the contribution of beam end rotation dropped to 54%, while that of joint distortion eventually increased to 30%.

Contribution patterns for the configuration 2 specimens generally seemed analogous to those of the configuration 1 specimens, but joint distortion contributions in all configuration 2 specimens were limited to just above 10%. Contributions of beam end rotation in PC2 and PC2-T, again mostly affected by joint opening, were maintained between approximately 62% and 79% within the entire drift ratio range, while the beam end rotation contribution in C-RC2 went as high as

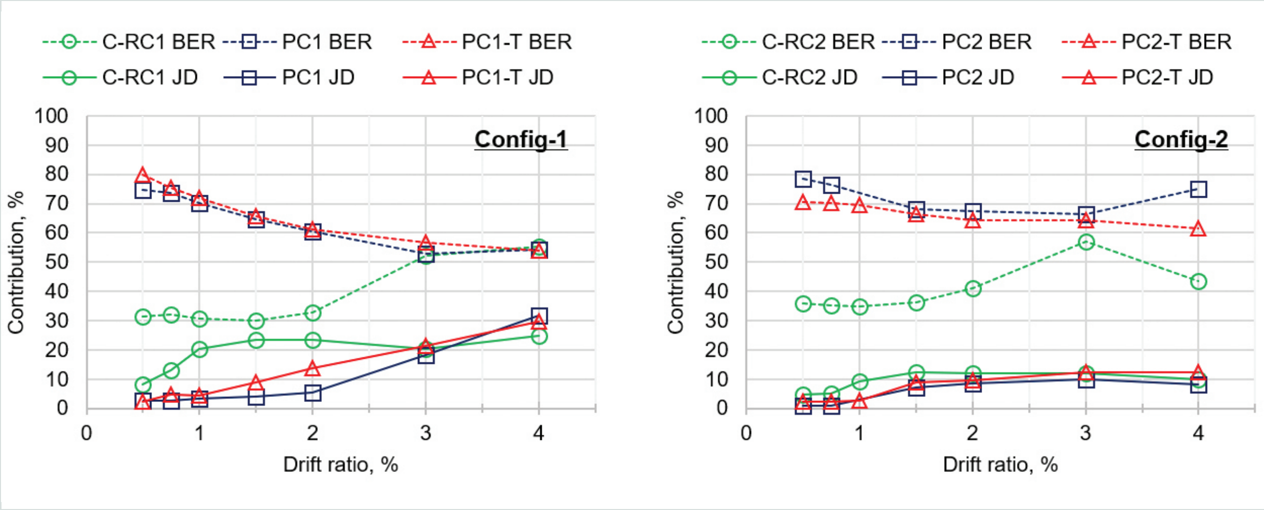

Figure 10. Contributions of beam end rotation (BER) and joint distortion (JD) to the total drift ratio in the positive direction. Note: Config-1 = specimens with 500 × 500 mm column and 400 × 650 mm beam configuration; Config-2 = specimens with 700 × 700 mm column and 500 × 700 mm beam configuration; C-RC1 = conventional reinforced concrete specimen with Config-1 dimensions; C-RC2 = conventional reinforced concrete specimen with Config-2 dimensions; PC1 = precast concrete specimen with Config-1 dimensions; PC1-T = precast concrete specimen with prestressed tendons and Config-1 dimensions; PC2 = precast concrete specimen with Config-2 dimensions; PC2-T = precast concrete specimen with prestressed tendons and Config-2 dimensions. 1 mm = 0.0394 in.

57%. Considering the similarity between the two precast concrete specimens (in configuration 1 and configuration 2), the existence of the prestressing tendons appeared to have no effect on the deformation contribution patterns.

Lateral stiffness and stiffness degradation

All precast concrete specimens exhibited apparent pinching behavior and resulting stiffness variations associated with slip at the connection. **Figure 11** shows a typical lateral force-to-drift ratio relationship of the precast concrete specimens during load reversal. To better investigate the pinching behavior, two stiffness values K_1 and K_2 were considered. K_1 indicates lower stiffness of the lateral response due to slip, whereas K_2 indicates increased stiffness after the slip. An intersection of the K_2 slope line and the horizontal axis is denoted as O', where O' corresponds to the effective slip displacement and its abscissa from the origin can be defined as an effective slip Δ_{slip} in each direction (positive and negative). Lateral stiffness of the precast concrete specimens and its degradation under cyclic loading were compared with the stiffness of the reinforced concrete specimens.

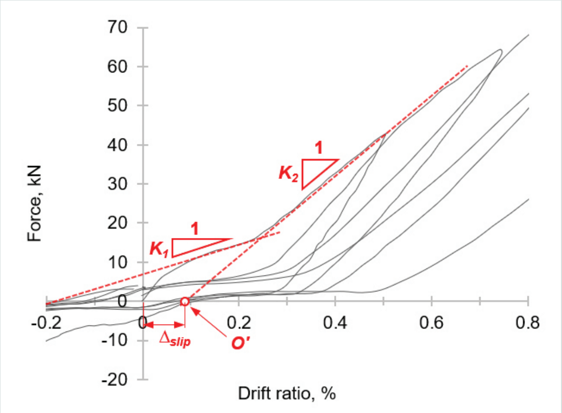

Figure 11. Stiffness variation of the precast concrete specimens due to slip during load reversals. Note: K_1 = lower stiffness of lateral response due to slip; K_2 = increased stiffness after slip; O' = point corresponding to effective slip displacement; Δ_{slip} = effective slip. 1 kN = 0.225 kip.

Figure 12 presents lateral secant stiffness of the specimens in the first cycle to each target drift. To estimate the secant stiffness of reinforced concrete specimens, the slope from the origin to the peak load point was calculated at each drift. For the precast concrete specimens, the point corresponding to effective slip displacement O' from Fig. 11 was used as a reference in each direction to minimize the effect of initial slip. In Fig. 12, C-RC1 shows a symmetric stiffness degradation pattern. Its initial stiffness reached 5000 kN/m (342.6 kip/ft), but with increased drift ratio the stiffness degraded rapidly to only 20% of the initial value at 5% drift ratio. Initial secant stiffness of PC1 was about half that of C-RC1; however, PC1 showed a much lower stiffness degradation rate, which in turn greatly reduced the stiffness gap between the two specimens at 5% drift ratio. Compared with PC1, PC1-T attained higher secant stiffness—as high as 3000 kN/m (205.6 kip/ft) in the positive direction—with the help of the prestressing tendons. The stiffness of PC1-T eventually became equivalent to that of C-RC1, from a drift ratio of 3% in the positive direction.

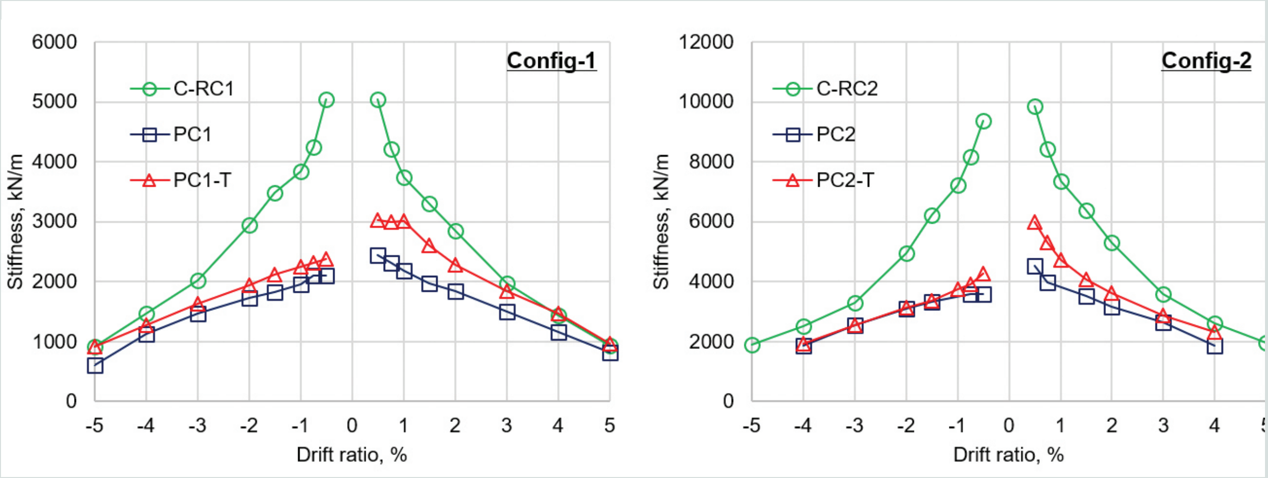

Figure 12. Lateral secant stiffness of beam-to-column connection specimens. Note: Config-1 = specimens with 500 × 500 mm column and 400 × 650 mm beam configuration; Config-2 = specimens with 700 × 700 mm column and 500 × 700 mm beam configuration; C-RC1 = conventional reinforced concrete specimen with Config-1 dimensions; C-RC2 = conventional reinforced concrete specimen with Config-2 dimensions; PC1 = precast concrete specimen with Config-1 dimensions; PC1-T = precast concrete specimen with prestressed tendons and Config-1 dimensions; PC2 = precast concrete specimen with Config-2 dimensions; PC2-T = precast concrete specimen with prestressed tendons and Config-2 dimensions. 1 mm = 0.0394 in.; 1 kN/m = 0.0685 kip/ft.

According to Fig. 12, the configuration 2 specimens were twice as stiff as the configuration 1 specimens, but their degradation patterns were quite similar. C-RC2 initially had much higher secant stiffness than the precast concrete specimens, but it decreased much more rapidly. Due to the prestressing effect, PC2-T recorded higher stiffness than PC2, by about 32% at 0.5% drift in the positive direction.

To assess how prestressing can affect the lateral stiffness of precast concrete specimens during slip, ratios of the two stiffness values K_1/K_2 were estimated from the first loading cycle to each target drift; they are compared in **Fig. 13**. The prestressing tendons started to make a clear difference in the stiffness ratios from a drift ratio of ±0.75%. Regardless of specimen configuration, the specimens without tendons mostly recorded stiffness ratios below 0.1 at drift ratios beyond 0.75% in both directions. The prestressed specimens, however, showed higher stiffness ratios—above 0.35 at low drift ratios—and retained at approximately 0.2 even at approximately 4% to 5% drift ratios, with gradual decreasing rates. The K_1/K_2 result in Fig. 13 reveals that although all precast concrete specimens inevitably experienced slip-induced, low lateral stiffness during load reversals (Fig. 6 and 8), this can be mitigated to some extent by the prestressing force acting through the joint, which provided extra lateral stiffness throughout testing.

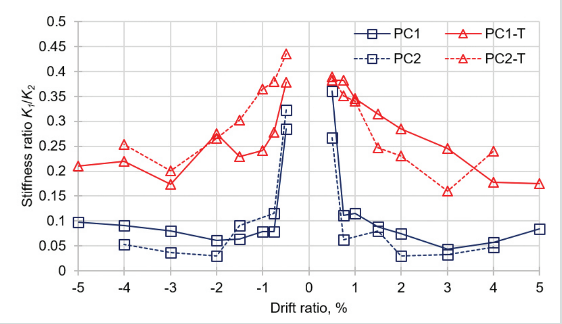

Figure 13. Effect of the prestressed tendons on stiffness ratio variations. Note: K_1 = lower stiffness of lateral response due to slip; K_2 = increased stiffness after slip; PC1 = precast concrete specimen with Config-1 dimensions; PC1-T = precast concrete specimen with prestressed tendons and Config-1 dimensions; PC2 = precast concrete specimen with Config-2 dimensions; PC2-T = precast concrete specimen with prestressed tendons and Config-2 dimensions.

Hysteretic energy dissipation

Figure 14 compares the overall energy dissipation capabilities of the beam-to-column connections up to the 4% drift loading cycle. Areas enclosed by lateral force-displacement curves of all three cycles were added to calculate the amount of cumulative energy dissipation. With increased component sizes, configuration 2 specimens dissipated much more energy than did the configuration 1 specimens. In both configurations, however, the reinforced concrete specimens generally possessed better energy dissipation capability than the precast concrete specimens. The cumulative energy dissipated by C-RC1 up to 4% drift ratio was 168.7 kN-m (124.4 kip-ft), about 1.83 times greater than that of PC1-T (92 kN-m [67.9 kip-ft]). An even greater difference, more than three times greater, was reported between C-RC2 (394 kN-m [290.6 kip-ft]) and PC2-T (124.2 kN-m [91.6 kip-ft]) at a 4% drift ratio. The high energy dissipation in the reinforced concrete specimens can be explained by a combination of two main factors: the yield strength of the D29 steel bars was much greater than their design strength and distributed damage due to a strong steel-to-concrete bond in the monolithic connections,

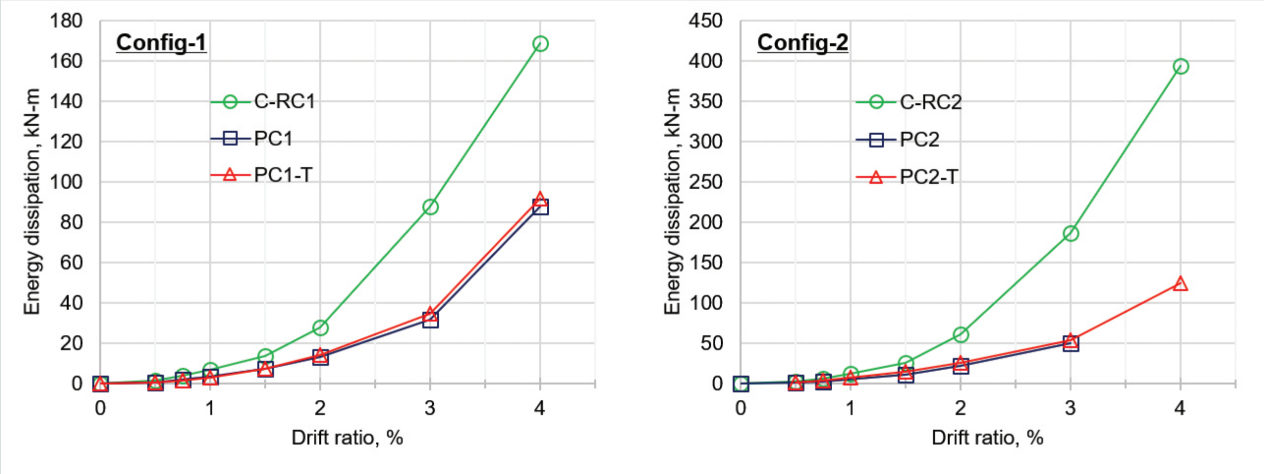

Figure 14. Cumulative energy dissipated by the beam-to-column connection specimens. Note: Config-1 = specimens with 500 × 500 mm column and 400 × 650 mm beam configuration; Config-2 = specimens with 700 × 700 mm column and 500 × 700 mm beam configuration; C-RC1 = conventional reinforced concrete specimen with Config-1 dimensions; C-RC2 = conventional reinforced concrete specimen with Config-2 dimensions; PC1 = precast concrete specimen with Config-1 dimensions; PC1-T = precast concrete specimen with prestressed tendons and Config-1 dimensions; PC2 = precast concrete specimen with Config-2 dimensions; PC2-T = precast concrete specimen with prestressed tendons and Config-2 dimensions. 1 mm = 0.0394 in.; 1 kN-m = 0.738 kip-ft.

which enabled stable and wide hysteresis loops. Conversely, the precast concrete specimens showed relatively more limited energy dissipation because of the good agreement between actual and design strengths of the ductile rods as well as the pinched behavior from reduced hysteresis loop areas. The cumulative energy dissipated by PC1 up to a 4% drift ratio was 87.9 kN-m [64.8 kip-ft], which indicates that prestressing tendons did not have a dramatic impact on the energy dissipation capability of the connection system (similar to the cases of PC2 and PC2-T, with up to a 3% drift ratio as shown in Fig. 14).

Tensile strains in longitudinal reinforcement

To help understand the flexural resistance mechanism of the specimens, tensile strains of the main longitudinal reinforcement were investigated. The D29 bars at the beam-to-column interface were selected for the reinforced concrete specimens, and the ductile rods and threaded bars were selected for the precast concrete specimens. **Figure 15** displays the peak tensile strains ε_{pk} of each reinforcement normalized by the correspond-

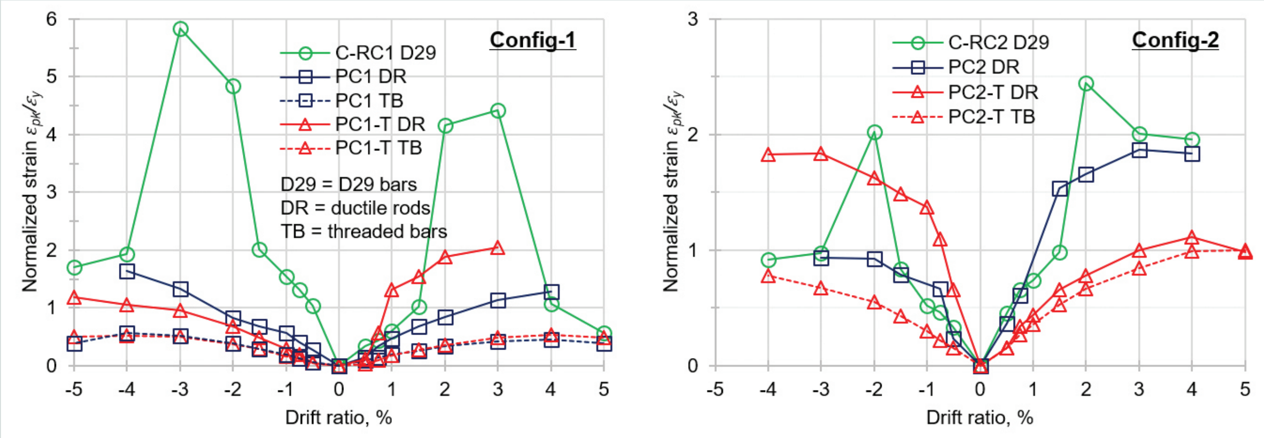

Figure 15. Normalized strains of longitudinal reinforcement. Note: Config-1 = specimens with 500 × 500 mm column and 400 × 650 mm beam configuration; Config-2 = specimens with 700 × 700 mm column and 500 × 700 mm beam configuration; C-RC1 = conventional reinforced concrete specimen with configuration 1 dimensions; C-RC2 = conventional reinforced concrete specimen with Config-2 dimensions; PC1 = precast concrete specimen with Config-1 dimensions; PC1-T = precast concrete specimen with prestressed tendons and Config-1 dimensions; PC2 = precast concrete specimen with Config-2 dimensions; PC2-T = precast concrete specimen with prestressed tendons and Config-2 dimensions; ε_{pk} = peak tensile strains; ε_y = yield strain. 1 mm = 0.0394 in.

ing yield strain ε_y. The graphs in Fig. 15 show somewhat large variations, but there is an overall increasing trend with the increment of imposed drift. For both configurations, the D29 bars and ductile rods (designated as the yielding components in the reinforced concrete and precast concrete specimens, respectively) yielded within a drift range of approximately 0.5% to 3%, a bit earlier than the yield drifts d_y determined globally in Table 4. Normalized strains of the threaded bars did not exceed unity, revealing that they all remained in the elastic range during testing. Despite some variation, the strain data in Fig. 15 confirm that the ductile rods were indeed functioning as the yielding component of the proposed connection system, in accordance with the intended resistance mechanism.

Prestressing forces

The prestressing forces of the tendons in PC1-T and PC2-T were continuously measured during testing. **Figure 16** shows the average measurements from the load cells. Prestressing forces of the two specimens varied cyclically and increased incrementally with applied drift ratio. Both forces started from around 80 kN (18 kip) and then reached more than 130 kN (29 kip) at 5% drift ratio (Fig. 16). The maximum forces in the tendons corresponded to 67.5% and 70.5% of their measured tensile strength (1893 MPa [275 ksi]) in PC1-T and PC2-T, respectively. Contribution of the tendons to the flexural strength was about 18.1% and 14.5% of the maximum force for PC1-T and PC2-T, respectively. The contribution of the tendons was maintained below 25% of the flexural strength at the joint section, so they satisfied section 18.6.3.5(c) of ACI 318-19.[20] The tendons in PC1-T provided an overall stable prestressing force throughout testing, with only 1.9% loss compared with its initial value. In PC2-T, however, the prestressing force dropped as low as 71.9 kN (16.2 kip) (an 11.2% loss) when the specimen was deformed by approximately 4% to 5% drifts in the negative direction. This higher force reduction could be associated with the cracking that occurred along the threaded bars. As the threaded bars were not fully able to carry the compressive forces due to bond failure, this may have imposed higher compressive force demands on the adjacent tendons, reducing their prestressing forces.

Performance evaluation by acceptance criteria of ACI 374.1-05

The acceptance criteria of ACI 374.1-05[22] were applied to examine the adequacy of using the ductile rod connection system as an effective lateral-force-resisting component in high seismic regions. For the third loading cycle at a drift ratio not less than 3.5%, ACI 374.1-05[22] requires the following:

- The peak lateral force of the loading cycle is not less than 75% of the maximum force capacity of the specimen in the same direction.
- The ratio of energy dissipated by the hysteretic loop to the area of circumscribing parallelograms is not less than ⅛ (12.5%).
- The secant stiffness between drift ratios of ±0.35% is not less than 5% of the stiffness at the initial drift ratio.

In this study, the test results of the configuration 1 specimens, which completed the full loading cycles of ±4% drift ratio, were used. (The configuration 2 specimens were excluded from the evaluation. PC2 abruptly lost its load-carrying capacity after reaching the first cycle at the ±4% drift ratio and although PC2-T completed its full loading cycles up to ±4% drift ratio, it did not properly demonstrate its performance due to bond failure of the threaded bars.)

Figure 17 shows a seismic performance evaluation for the configuration 1 specimens (that made it to 4% drift ratio)

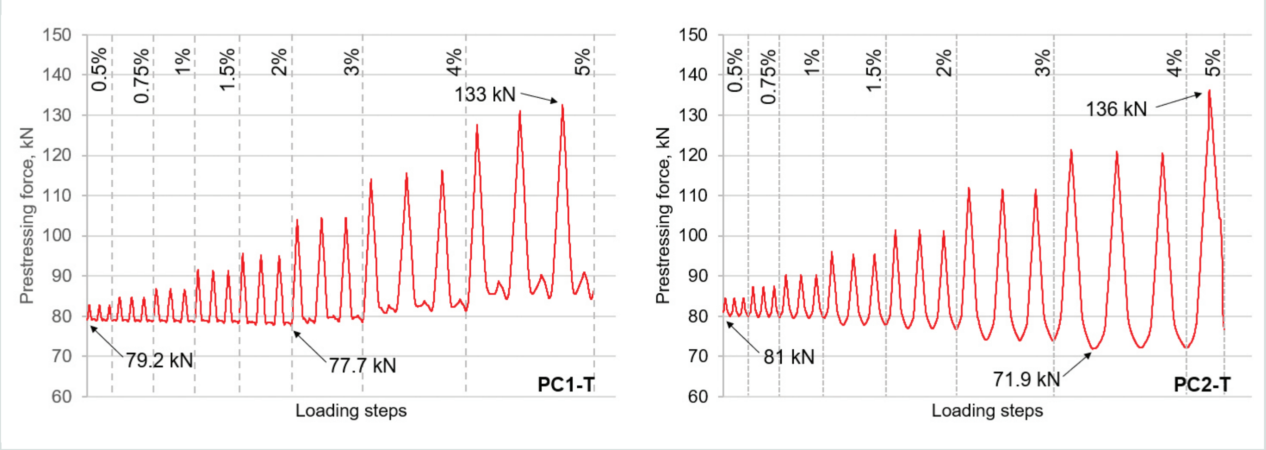

Figure 16. Average prestressing forces of the tendons in PC1-T and PC2-T. Note: PC1-T = precast concrete specimen with prestressed tendons and Config-1 dimensions; PC2-T = precast concrete specimen with prestressed tendons and Config-2 dimensions. 1 kN = 0.225 kip.

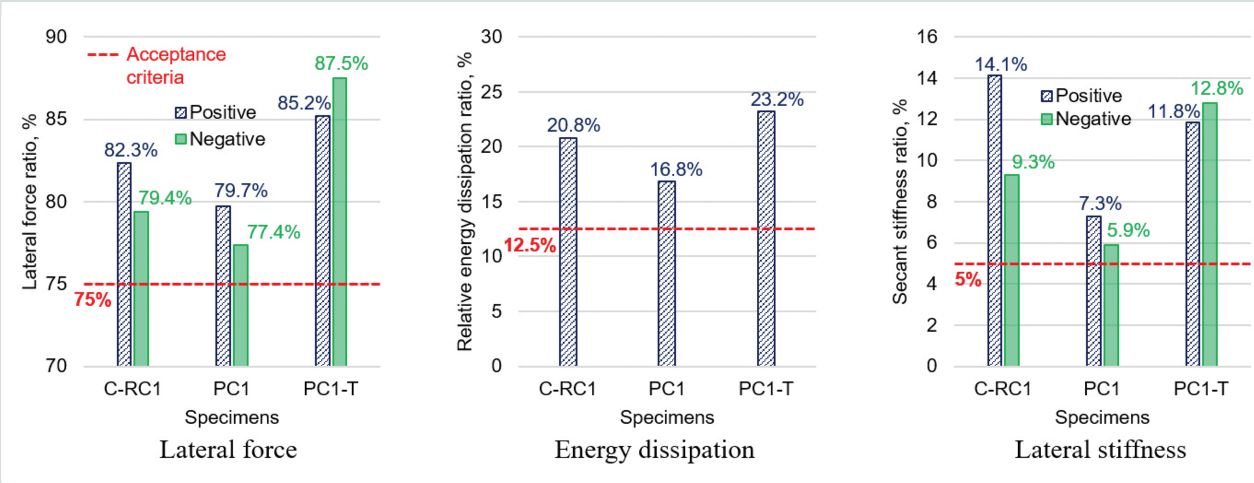

Figure 17. Seismic performance evaluation for the configuration 1 specimens according to ACI 374.1-05. Note: ACI = American Concrete Institute; Config-1 = specimens with 500 × 500 mm column and 400 × 650 mm beam configuration; C-RC1 = conventional reinforced concrete specimen with Config-1 dimensions; C-RC2 = conventional reinforced concrete specimen with Config-2 dimensions; PC1 = precast concrete specimen with Config-1 dimensions; PC1-T = precast concrete specimen with prestressed tendons and Config-1 dimensions. 1 mm = 0.0394 in.

with respect to lateral force, energy dissipation, and lateral stiffness. Among the three specimens, PC1 exhibited the overall lowest performance but still satisfied the three acceptance criteria. With the prestressing tendons, PC1-T showed enhanced performance in all aspects. The lateral force, energy dissipation, and secant stiffness ratios of PC1-T increased to more than 85%, 23%, and 12%, respectively, achieving outcomes comparable to or better than C-RC1. The seismic performance evaluation for the precast concrete specimens demonstrates that they, as part of a whole frame, have sufficient lateral resistance and energy dissipation capability to prevent undesirable oscillations or excessive displacements after a seismic event.

Conclusion

This study introduces a ductile rod exterior connection system for precast concrete components and presents experimental results of seven full-scale exterior beam-to-column connection subassemblies tested under reversed cyclic loading. Different design parameters—ductile rod size, presence of prestressing, beam flexural capacity, and joint shear capacity—were applied to the five precast concrete specimens, and their responses were compared with two monolithic reinforced concrete specimens. The main findings and lessons learned from the current study can be summarized as follows:

- The precast concrete specimens accurately achieved their expected moment capacities in both configuration 1 (PC1 and PC1-T) and configuration 2 (PC2 and PC2-T). In most cases, the moment capacities of the precast concrete specimens were reached by 4% drift ratio, about 1% behind otherwise comparable reinforced concrete specimens.

- The ductile rods embedded in the joint governed the flexural response of the connections through inelastic push-in and pullout actions. Flexural rotation at the end of the precast concrete beam contributed to a majority of the total lateral deformation.

- The precast concrete specimens showed lower lateral stiffness than the reinforced concrete specimens. Conversely, stiffness degradation with an increase in drift ratio progressed at a much slower pace in the precast concrete specimens. Furthermore, all precast concrete specimens exhibited clear pinching behavior during load reversals, which can be alleviated by providing prestressing tendons.

- The precast concrete specimens exhibited different damage mechanisms depending on their connection design. PC1 and PC1-T, which had the smaller column size, sustained substantial joint damage associated with pullout of the ductile rods. PC1S failed prematurely in the early loading stage due to inadequate rod design. The increased number of ductile rods in the configuration 2 precast concrete specimens induced high force demand on the threaded bars and a resulting bond failure.

- The aforementioned damage mechanisms provide important insight into the design of the proposed connection system. Sufficient size of the column is needed to prevent pullout or shear failure of the joint (collapse prevention). To avoid undesirable failure modes and damage patterns, it is crucial to carefully consider all connection details and their consequences, including the size, shape, and number of ductile rods. Last, a sufficient development length (or continuity) needs to be secured for the threaded bar to enable the precast concrete specimens to fully exploit their performance.

- Despite the severe joint damage, the configuration 1 precast concrete specimens showed satisfactory seismic performance at a high drift ratio. They fulfilled the acceptance criteria of ACI 374.1-05[22] in terms of lateral strength, relative energy dissipation, and lateral stiffness.

Finally, it is worth noting that use of the developed exterior connection system is more suitable for industrial buildings. If more than two beams are connected to one column location using the ductile rods, interference or congestion of the ductile rods can be expected to occur at the joint. In industrial buildings, the beams can be connected at different locations (that is, at varying heights) of the column or with different methods (for example, by using corbels in one direction) to avoid this issue.

Acknowledgments

This project was funded by the National Research Foundation of Korea (no. 2018R1D1A1B06044752). Pretension bolt rigid connection specimens were provided by Euro Engineering Co. Ltd. in Korea. The authors would like to acknowledge the engineers of Euro Engineering Co. Ltd. for their helpful discussion and former graduate students Judong Lee at Seoul National University in Korea and Texas A&M University in College Station for his participation in structural testing in Korea and Jae Ho Shin at the University of Illinois Urbana-Champaign for his participation in data reduction. The views expressed are those of the authors and do not necessarily represent those of the sponsors or other participants.

References

1. Kim, Jin-Won, Choel-Ho Lee, and Thomas H.-K. Kang. 2014. “Shearhead Reinforcement for Concrete Slab to Concrete-Filled Tube Column Connections.” *ACI Structural Journal* 111 (3): 629–638. https://doi.org/10.14359/51686623.

2. Lim, Woo-Young, Thomas H.-K. Kang, and Sung-Gul Hong. 2016. “Cyclic Lateral Testing of Precast Concrete T-Walls in Fast Low-Rise Construction.” *ACI Structural Journal* 113 (1): 179–189. https://doi.org/10.14359/51688200.

3. Pillai, S. U., and D. W. Kirk. 1981. “Ductile Beam-Column Connection in Precast Concrete.” *ACI Journal Proceedings* 78 (6): 480–487. https://doi.org/10.14359/10926.

4. Bhatt, Prabhakara, and D. W. Kirk. 1985. “Tests on an Improved Beam Column Connection for Precast Concrete.” *ACI Journal Proceedings* 82 (6): 834–843. http://doi.org/10.14359/10395.

5. Cheok, Geraldine S., and H. S. Lew. 1990. “Performance of ⅓-Scale Model Precast Concrete Beam–Column Connections Subjected to Cyclic Inelastic Loads.” NISTIR (NIST Interagency/Internal Report) 4433. Gaithersburg, MD: NIST (National Institute of Standards and Technology). https://doi.org/10.6028/NIST.IR.4433.

6. Cheok, Geraldine S., and H. S. Lew. 1991. “Performance of ⅓-Scale Model Precast Concrete Beam–Column Connections Subjected to Cyclic Inelastic Loads. Report No. 2.” NISTIR 4589. Gaithersburg, MD: NIST. https://doi.org/10.6028/NIST.IR.4589.

7. Cheok, Geraldine S., and William C. Stone. 1993. “Performance of ⅓-Scale Model Precast Concrete Beam–Column Connections Subjected to Cyclic Inelastic Loads. Report No. 3.” NISTIR 5246. Gaithersburg, MD: NIST. https://doi.org/10.6028/NIST.IR.5246.

8. Cheok, Geraldine S., and William C. Stone. 1994. “Performance of ⅓-Scale Model Precast Concrete Beam–Column Connections Subjected to Cyclic Inelastic Loads. Report No. 4.” NISTIR 5436. Gaithersburg, MD: NIST. https://doi.org/10.6028/NIST.IR.5436.

9. Priestley, Michael John Nigel. 1991. “Overview of PRESSS Research Program.” *PCI Journal* 36 (4): 50–57. https://doi.org/10.15554/pcij.07011991.50.57.

10. Nakaki, Suzanne D., and Robert E. Englekirk. 1991. “PRESSS Industry Seismic Workshops: Concept Development.” *PCI Journal* 36 (6): 54–61. https://doi.org/10.15554/pcij.09011991.54.61.

11. Nakaki, Suzanne D., Robert E. Englekirk, and Juergen L. Plaehn. 1994. “Ductile Connectors for a Precast Concrete Frame.” *PCI Journal* 39 (5): 46–59. https://doi.org/10.15554/pcij.09011994.46.59.

12. Englekirk, Robert E. 1995. “Development and Testing of a Ductile Connector for Assembling Precast Concrete Beams and Columns.” *PCI Journal* 40 (2): 36–51. https://doi.org/10.15554/pcij.03011995.36.51.

13. Day, Stephen. 1999. “Cyclic Load Testing of Precast Hybrid Frame Moment-Resisting Connections.” MSc thesis, Department of Civil and Environmental Engineering, University of Washington, Seattle, WA.

14. Kim, Jubum. 2000. *Final Report on Testing of Hybrid Frame Corner Beam-Column Sub-assembly with Continuous Post-tensioning Steel*. University of Washington, Seattle, WA: Structural Research Laboratory.

15. Chang, Barbara, Tara C. Hutchinson, Xiang Wang, and Robert E. Englekirk. 2013. “Experimental Seismic Performance of Beam–Column Subassemblies Using Ductile Embeds.” *Journal of Structural Engineering* 139 (9): 1555–1566. https://doi.org/10.1061/(ASCE)ST.1943-541X.0000628.

16. ASTM Subcommittee F16.02. 2012. *Standard Specification for Structural Bolts, Alloy Steel, Heat Treated, 150 ksi Minimum Tensile Strength*. ASTM A490. West Conshohocken, PA: ASTM International. https://doi.org/10.1520/A0490-12.

17. AISC (American Institute of Steel Construction). 2016. *Specification for Structural Steel Buildings*. Chicago, IL: AISC.

18. AIK (Architectural Institute of Korea). 2016. *Korean Building Code—Structural*. [In Korean.] Seoul, Korea: AIK.

19. Englekirk, Robert E. 2003. *Seismic Design of Reinforced and Precast Concrete Buildings*. Hoboken, NJ: John Wiley & Sons.

20. ACI (American Concrete Institute) Committee 318. 2019. *Building Code Requirements for Structural Concrete (ACI 318-19) and Commentary (ACI 318R-19)*. Farmington Hills, MI: ACI.

21. Joint ACI-ASCE (American Society of Civil Engineers) Committee 352. 2002. *Recommendations for Design of Beam–Column Joints in Monolithic Reinforced Concrete Structures*. ACI 352R-02. Farmington Hills, MI: ACI.

22. ACI Committee 374. 2005. *Acceptance Criteria for Moment Frames Based on Structural Testing and Commentary*. ACI 374.1-05. Farmington Hills, MI: ACI.

23. ACI Committee 374. 2013. *Guide for Testing Reinforced Concrete Structural Elements under Slowly Applied Simulated Seismic Loads*. ACI 374.2 R-13. Farmington Hills, MI: ACI.

24. Kim, Jaehong, and James M. LaFave. 2012. "Simplified Approach to Joint Shear Behavior Prediction of RC Beam–Column Connections." *Earthquake Spectra* 28 (3): 1071–1096. https://doi.org/10.1193/1.4000.

25. Foltz, Raymond R., James M. LaFave, and Deuckhang Lee. 2022. "Seismic Performance of a Structural Concrete Pile–Wharf Connection Before and After Retrofit." *Structures* 38: 874–894. https://doi.org/10.1016/j.istruc.2022.02.042.

Notation

A_{bolt} = cross-sectional area

A_j = effective joint area

A_{rod} = cross-sectional area of ductile rod

A_{thr} = cross-sectional area of high-strength threaded bar

d = effective beam depth

d_{pk} = drift ratio at peak moment

d_{rod} = distance from beam's top face to centroid of bottom

d'_{rod} = distance from top of beam face to top ductile rods

d_u = ultimate drift ratio

d_y = drift ratio at yield

D_{bolt} = diameter of high-tension bolt

f'_c = compressive strength of concrete

$f_{eff,ten}$ = effective prestressing value of tendons measured on day of testing

$f_{u,ten}$ = ultimate stress of tendons

f_y = yield strength

$f_{y,h}$ = measured yielding stress of stirrups

$f_{y,rod}$ = measured yielding stress of ductile rods

$f_{y,thr}$ = measured yielding stress of threaded bars

F_{nt} = nominal tensile strength

h_c = distance between column supports in test setup

K = coefficient of torque

K_1 = lower stiffness of lateral response due to slip

K_2 = increased stiffness after slip

M_{exp} = expected moment strength based on measured material properties

M_n = nominal moment capacity

M_{pk} = measured peak moment

n_{rod} = number of ductile rods

n_{thr} = number of high-strength threaded bars

N_{bolt} = tension in bolt induced by tightening

O' = point corresponding to effective slip displacement

T = torque

V = joint shear force

V_{col} = column shear

V_{exp} = expected shear strength at joint with measured material properties

V_j = shear force demand on joint

$V_{j,pk}$ = measured peak shear strength of joint

V_n = nominal shear strength

α = stress multiplier for longitudinal reinforcement

γ = coefficient for connection type

Δ_{slip} = effective slip

ε_{pk} = peak tensile strains

ε_y = yield strain

μ_d = displacement ductility

ϕ_1 = resistance factor that conservatively considers uncertainties in load and effective (reduced) tension area of threaded portion

ϕ_2 = resistance factor for tension yielding in gross section

About the Authors

Donghyuk Jung, PhD, is an assistant professor at Korea University in Seoul, Korea. Before that, he was an assistant professor at Pusan National University in Busan, Korea.

Thomas H.-K. Kang, PhD, PE, is a professor of structural engineering and director of the Engineering Education Innovation Center at Seoul National University in Korea. He has also been an adjunct professor at the University of Illinois Urbana-Champaign.

Dong Joo Lee, MS, is a designer/engineer at Hanssem Co. Ltd. in Korea. She received her master of science degree from Seoul National University and bachelor of architecture degree from Hongik University in Korea.

Sanghee Kim, PhD, is an assistant professor at Kyonggi University in Suwon, Korea. Before that he was a postdoctoral researcher at Seoul National University, where he received his PhD.

James M. LaFave, PhD, PE, is a professor in the Department of Civil and Environmental Engineering at the University of Illinois Urbana-Champaign.

Abstract

The seismic performance of a ductile rod system for exterior precast concrete beam-to-column connections was experimentally evaluated. Five full-scale precast concrete beam-to-column subassemblies connected with ductile rods were fabricated, considering various aspects (ductile rod size, prestressing, and flexural/shear capacities). Lateral cyclic loading tests were conducted for the precast concrete connections along with two monolithic reinforced concrete connections. Despite their relatively lower lateral stiffness, most precast concrete connections showed sufficient moment capacities with peak moments at approximately 3% to 4% interstory drifts. The prestressing tendons were effective at enhancing moment and shear strengths of the precast concrete connections, as well as in reducing slip of the ductile rods. The precast concrete specimens generally showed satisfactory seismic performance, fulfilling acceptance criteria specified by the American Concrete Institute. The test results demonstrated that careful considerations are required in the design of ductile rods and high-strength threaded bars to induce stable flexural responses of the precast concrete connections.

Keywords

Ductile rod connection system, exterior beam-to-column connection, lateral cyclic loading tests, prestressing, seismic performance.

Review policy

This paper was reviewed in accordance with the Precast/Prestressed Concrete Institute's peer-review process. The Precast/Prestressed Concrete Institute is not responsible for statements made by authors of papers in *PCI Journal*. No payment is offered.

Publishing details

This paper appears in *PCI Journal* (ISSN 0887-9672) V. 68, No. 1, January–February 2023, and can be found at https://doi.org/10.15554/pcij68.1-03. *PCI Journal* is published bimonthly by the Precast/Prestressed Concrete Institute, 8770 W. Bryn Mawr Ave., Suite 1150, Chicago, IL 60631.

Reader comments

Please address any reader comments to *PCI Journal* editor-in-chief Tom Klemens at tklemens@pci.org or Precast/Prestressed Concrete Institute, c/o *PCI Journal*, 8770 W. Bryn Mawr Ave., Suite 1150, Chicago, IL 60631.